THE PENNSYLVANIA STATE UNIVERSITY
SCHREYER HONORS COLLEGE

DEPARTMENT OF CIVIL AND ENVIRONMENTAL ENGINEERING

CAN META-SOIL ATTENUATE SEISMIC WAVES?

ALEXIS GAWELKO
SPRING 2019

A thesis
submitted in partial fulfillment
of the requirements
for a baccalaureate degree
in Civil Engineering
with honors in Civil Engineering

Reviewed and approved* by the following:

Parisa Shokouhi
Associate Professor of Engineering Science & Mechanics
Thesis Supervisor

Eric Donnell
Professor of Civil Engineering
Honors Adviser

* Signatures are on file in the Schreyer Honors College.

ABSTRACT

Stable and resilient civil infrastructure is a key to public safety. However, current structures are vulnerable to damage resulting from excessive ground motion caused by earthquakes or underground explosions. Traditionally, structures are built to withstand ground motion, but this design approach is costly and the risk of failure during very large events remains high. A fundamentally different approach is found in controlling the ground motion itself through engineering the soil to act as an acoustic metamaterial. Acoustic metamaterials are composites, often with a periodic substructure, that have the ability to control the propagation of elastic waves through scattering or local resonance mechanisms. Recently, advances in the understanding of metamaterials have allowed the creation of stop bands in wave transmission around the resonator's natural frequency. A graded array of low-frequency acoustic metamaterials provides the possibility to create targeted band-stops, effectively filtering out destructive ground motion. Numerical modeling is used to inform future experimental design to study this phenomenon at laboratory scale. Local resonators are modeled as spheres with a heavy metal core and a thin elastic coating. A sensitivity analysis is performed in order to inform the design of improved resonators. Then, alternative resonators are modeled as spheres with a heavy metal core and elastic columns made of plastic. The geometry and material properties of the resonators are varied in numerical simulations to optimize the frequency range and width of the band gaps. Similar resonators could be incorporated at full scale to create a seismic shield around critical structures.

TABLE OF CONTENTS

LIST OF FIGURES

LIST OF TABLES

Chapter 1

Introduction

Motivation

In January 2010, the Haiti earthquake caused damage to structures, roads, and over 294,000 homes. In total, the 7.0 magnitude earthquake caused approximately $8 billion in damage [1]. However, earthquakes do not only occur in Haiti. They occur in the United States, Japan, Chile, and all over the world. They occur in remote countries, crowded cities, and suburbs. Earthquakes are a global problem. The United States Geological Survey (USGS) Earthquake Hazard Program estimates that from 2000-2016 there were 31,759 earthquakes worldwide, causing 801,629 deaths [2]. Currently, hundreds of millions of people live in earthquake hazard areas, and billions of dollars of infrastructure are vulnerable, putting economies at risk as well [3].

Traditional earthquake and vibration engineering techniques have evolved greatly in the last few decades, however significant damage and fatalities still occur in seismic events. There are many different types of seismic waves and which has the greatest effect on a structure depends heavily on the site conditions. The two types of waves produced when an earthquake occur are body waves and surface waves. Body waves consist of P-waves and S-waves, as seen in *Figure 1*. P-waves are the fastest seismic waves, the first to reach a structure when an earthquake occurs. Like acoustic waves, the particles travel parallel to the direction of propagating energy. S-waves cause shearing deformations as they propagate, as their motion is perpendicular to the direction of propagation. Surface waves, consisting of Rayleigh waves and Love waves as shown in *Figure 2* are created from the interaction of body waves and the Earth's crust. They have the greatest effect at distances

further from the source of the earthquake and their magnitudes decrease exponentially with depth [3].

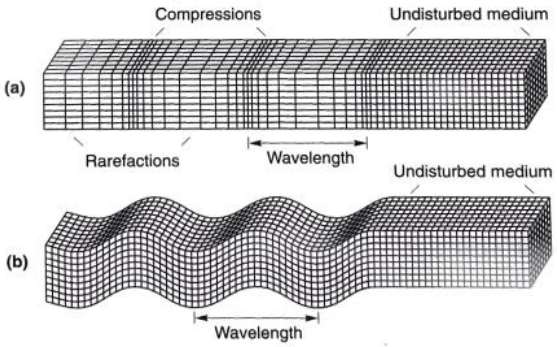

Figure 1 ***Deformations produced by body waves: (a) P-wave; (b) S-wave. Source: Geotechnical Earthquake Engineering by Kramer. Copyright 1993 by W.H. Freeman and Company***

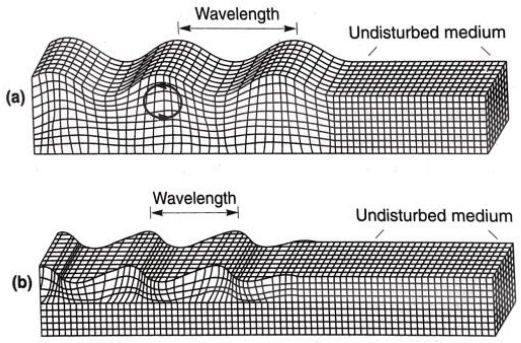

Figure 2 ***Deformations produced by surface waves: (a) Rayleigh wave; (b) Love wave. Source: Geotechnical Earthquake Engineering by Kramer. Copyright 1993 by W.H. Freeman and Company***

To counteract the damaging effects of earthquake waves, engineers use passive and active control systems. In a seismic event, passive control structures aim to consume part of the input energy and minimize structural damage. They are installed as energy dissipation or damping mechanism devices possessing certain stiffness and damping characteristics. Examples of passive control systems include metallic, friction, visco-elastic, viscous fluid dampers, tuned mass dampers, and tuned liquid dampers. Examples of various passive control systems are show in *Figure 3*. Base isolation is a form of passive control that includes inserting a low stiffness layer at the foundation of a structure in order to reduce its natural period in vibration. For the most part, these devices are simple to design and build, however they are only designed for one dynamic loading case. Therefore, these methods often fail to protect structures from all types and magnitudes of seismic waves. In addition, the foundation of a structure will usually still have a large horizontal displacement after an earthquake has occurred. This creates further issues involving the underground utilities that enter the structure through the foundation.

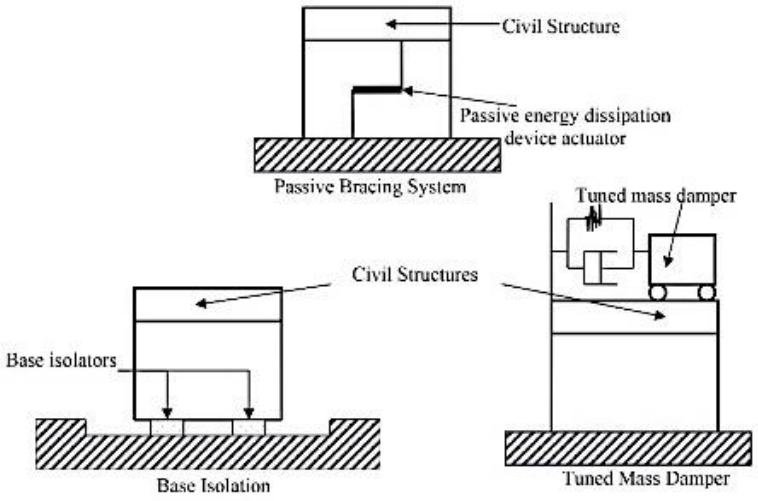

Figure 3 ***Passive control system examples. Source: Hadi (2017)***

Active systems are controllable, while passive control systems are not. They work by creating forces in the structure to counteract the energy of an applied dynamic loading. Some examples of active control systems include active tuned mass dampers and active bracing systems, as seen in *Figure 4*. Sensors placed throughout a structure measure amplitude and send records to a computer, which activates devices during a seismic event. A drawback to active systems is that they require a significant amount of power to run, which leads to extra costs. In addition, this external power supply cannot be interrupted during an earthquake event, or the system will not function. Active control devices are often complex to design and implement, and they are expensive to install and maintain.

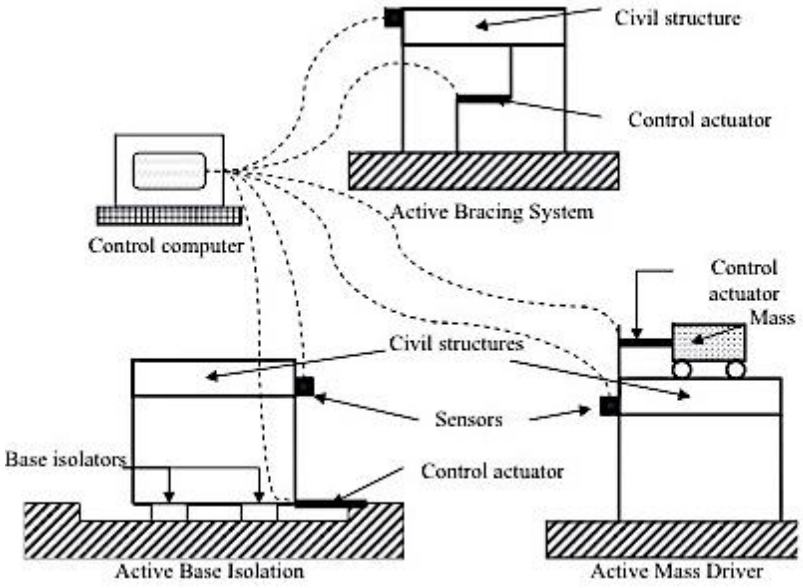

Figure 4 ***Active control system examples. Source: Hadi (2017)***

Semi-active control systems combine certain aspects of passive and active devices. Semi-active devices can absorb energy during an excitation, as passive devices do. Then, the system reacts to provide a force to the structure, acting as an active device. The drawbacks of these two methods still exist, although to a lesser extent [4].

Structures vary significantly in their reaction to a seismic event due to differences in geometric and material properties of the structure itself, soil and bedrock properties, type, direction, and magnitude of incident earthquake waves, and the effect of adjacent structures. A technique has not yet been implemented that has the potential to protect a wide variety of structures against a wide variety of seismic events. Current passive, active, and semi-active earthquake protection methods for structures are insufficient, as they are expensive and significant damage still occurs after ground shaking [4], [5].

Background

Recent research has focused on developing a fundamentally new approach, in which the ground motion itself is controlled to prevent dangerous waves from reaching a structure through the use of metamaterials. Metamaterials consist of composites with an engineered microstructure that can exhibit a negative effective dynamic mass density and elastic modulus. These unique properties can lead to the manipulation of elastic wave propagation. Phononic crystals and acoustic metamaterials have shown promising results in the manipulation of elastic wave propagation through Bragg scattering or local resonances. This field of research is fairly recent, only gaining traction within the last two decades [6]. Narayanamurti et al. (1979) demonstrated the first example of controlling high-frequency phonons through a superlattice in 1979 [7]. In 1995, the first physical demonstration of this phenomenon was conducted by Francisco Meseguer. Meseguer and his peers studied the wave-filtering properties of a sculpture in Madrid consisting of a periodic arrangement of steel tubes, as shown in *Figure 5*. For different frequencies of propagating waves, either constructive or destructive interferences occur. The destructive interferences are a result of scattering, and therefore cause the structure to exhibit band gaps [8].

Liu et al. (2000) presented a structure that attenuates bulk waves due to local resonance. A simple cubic crystal was modeled, consisting of an arrangement of heavy lead cores coated with silicone in an epoxy matrix, as seen in *Figure 6.* At the resonant frequencies of the inclusions, the center of mass of the metamaterial has a displacement that is out of phase with the acoustic wave, causing an effective negative dynamic mass density. Therefore, transmission gaps exist at these frequencies [9].

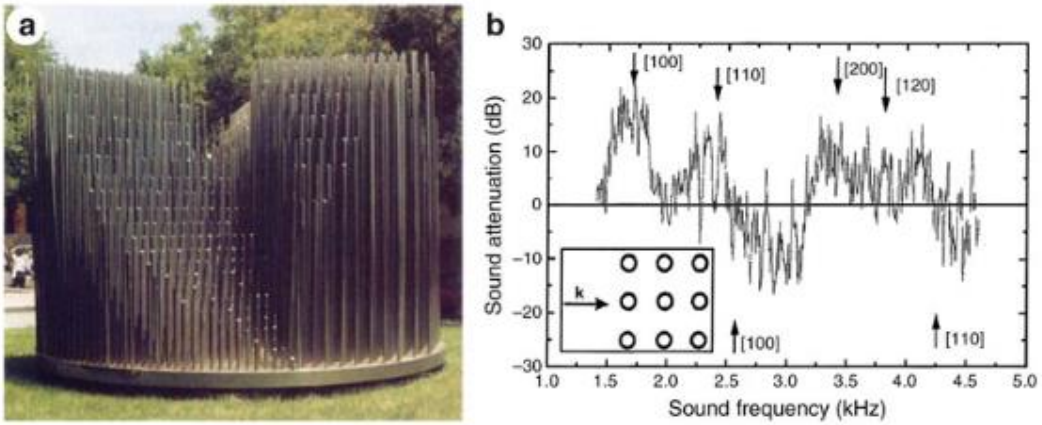

Figure 5 ***(a) Madrid sculpture, (b) Sound attenuation through sculpture. Source: Deymeir (2013)***

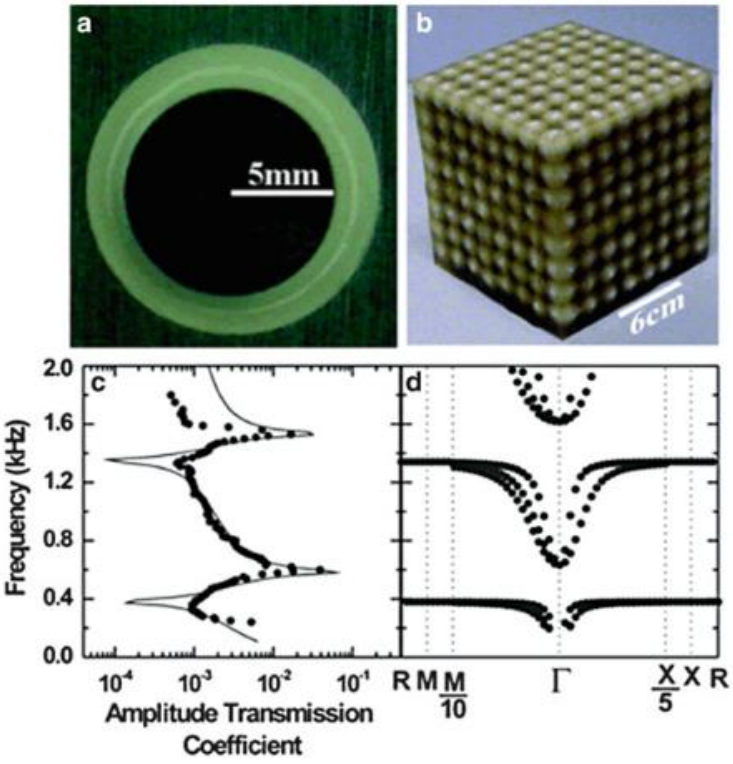

Figure 6 ***(a) Cross-section of a coated lead sphere, (b) a sonic crystal of 8x8 coated lead spheres, (c) Calculated (line) and measured (dots) amplitude transmission coefficient, (d) Band structure of crystal. Source: Deymeir (2013)***

The successful use of metamaterials to filter waves in acoustics provides a promising solution for seismic applications, as seismic waves can be described as inhomogeneous acoustic waves with various wavelengths on the order of hundreds of meters. Studies have predicted that metamaterials can even prevent the transmission of an incident wave at or near their natural frequency. Therefore, an array of metamaterials with different resonant frequencies has the potential to create wide band gaps and effectively filter out dangerous ground vibration. In the last decade, researchers have developed two methods for the manipulation of seismic waves using acoustic metamaterials: surface metamaterials and embedded resonators [10].

Resonators arranged on the surface of an elastic half-space such as the Earth's crust have the potential to protect critical infrastructure from seismic waves. Colombi et al. (2016) designed a seismic metawedge, consisting of vertical resonators in a graded arrangement from 1 to 14m, as seen in *Figure 7*. The resonance frequency range of the metawedge is 30-120 Hz, which is higher than most seismic waves. If the seismic waves propagate such that it reaches the shorter side of the metawedge first, much of the energy is reflected. This could cause serious damage to structures on the wrong side of the resonators. Rayleigh waves that propagate towards the taller grade of the metawedge are converted by the above-surface structure into bulk waves, traveling downwards and possibly underneath the structure of interest [11].

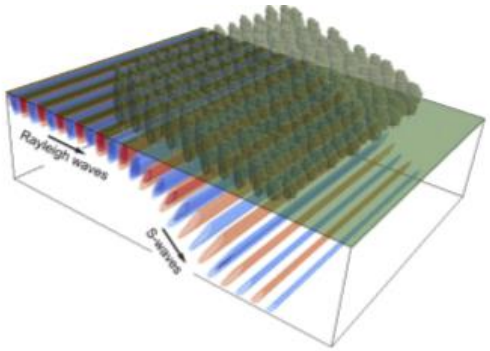

Figure 7 ***Conversion phenomena by resonant metawedge. Source: Colombi et al. (2016)***

Another study by Colombi et al. (2016) explored the possibility of trees in forests acting as a natural version of above-surface resonators. An experiment was carried out in a small forest consisting of mainly pine trees and a significant attenuation of surface waves was achieved at 30 to 45 Hz and 90 to 110 Hz. Next, the forest was modeled using vertical rods to represent trees. They found a bandgap from 32-40 Hz and from approximately 90-105 Hz. The forest works in a way similar to the metawedge, in that it converts surface waves to downwardly-propagating bulk waves, therefore creating a surface wave-free zone beneath the trees. They also found that a larger variation in the size and arrangement of trees produced a larger band gap [12].

While above-surface resonators have the potential to shield structures, they do so by reflecting or redirecting seismic waves. This could result in dangerous effects to structures on the wrong side of the surface resonators. In addition, a lot of space is needed to construct a metawedge and space may not be available in some areas, particularly in cities [10].

Xiang and Shi et al. (2012) took a different approach, creating a foundation that was itself a metamaterial. They designed a one-dimensional layered periodic foundation consisting of alternating rubber and reinforced concrete layers. First, a finite element model was built and S-waves were simulated. Band gaps were observed at 6.6-15.0 Hz and at 17.8-30.0 Hz, which includes the natural frequency of the frame built on top of the periodic structure. Resonance of the frame, which can be thought of as a critical structure to be protected, would result in serious damage. Therefore, the fact that this frequency cannot pass through the periodic foundation is ideal. Xiang and Shi et al. (2012) were also one of the first research groups to confirm modeling results for vibration attenuation experimentally using metamaterials. They built a scaled physical model consisting of a 1.5-ton specimen made of rubber and concrete layers bonded together with polyurethane glue. The specimen was tested using a biaxial shaking table and the seismogram from the 1975 Oroville earthquake. Results demonstrated that the periodic foundation was able to reduce

peak horizontal acceleration by up to 50% as compared to the control specimen without a layered foundation, but it was not able to reduce the vertical displacement of the structure on top of the foundation [4]. Xiang and Shi et al. (2012) effectively modeled and created a seismic isolator, however they did not attempt to analyze shifting or widening the frequency band gap produced by the periodic foundation.

Next, Shi and Huang (2013) considered a three-dimensional, three-component periodic foundation, composed of a unit cell with a cubic core and soft coating shell embedded in a concrete matrix. Through computational and numerical simulations, they confirmed that a higher core density, an increase in the elastic modulus of the coating layer, and an increase in the filling fraction all lead to a wider attenuation zone achieved by the metamaterial. They were able to produce a band gap as low as approximately 8-15 Hz, but only achieved 20-30% attenuation overall when their periodic foundation was numerically subjected to the same seismic waves generated by a past earthquake [13].

Another approach taken by researchers, which attempts to address the concern for space by embedding the resonators in the surface, is an arrangement of cylindrical inclusions or voids in the ground that utilize scattering effects to dissipate seismic waves. Kim and Das (2012) developed equations to find the negative effective shear modulus of a metamaterial, allowing a method of design producing a specific band gap. They concluded that seismic surface waves can be attenuated through the use of Helmholtz resonators, or an array of cylinders with holes in the side [14]. The design of their meta-cylinder is shown in *Figure 8*.

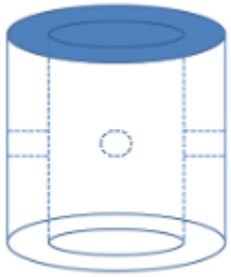

Figure 8 ***Hemholtz resonator design. Source: Kim and Das (2012)***

Huang and Shi (2013) conducted a numerical simulation to study the periodic nature of two-dimensional row piles, or embedded surface resonators. Concrete piles were designed and modeled, and factors that influenced the band gaps achieved by the metastructure were analyzed. They concluded that an increase in the number of rows of piles, a larger filling fraction (the volume ratio of pile to surrounding material) and softer soil all increased the band gap width. However, the piles failed to isolate vibrations outside of the band gap [15].

Cheng and Shi (2013) conducted another study on the attenuation zones of periodic structures. Two component rubber-concrete and rubber-steel cylindrical inclusions were modeled. The higher density of the steel core resulted in a lower band gap frequency and wider attenuation zone than the concrete core. They also found that a larger core radius and smaller periodic constant increase both the lower and upper frequency of the band gap. Three-component cylindrical inclusions were also analyzed. Larger core radii and smaller coating thickness were found to be favorable in widening the band gap based on local resonance of the inclusions [16].

Brulé et al. (2014) advanced the study of embedded surface scatterers by creating a large-scale experiment to investigate the effectiveness of cylindrical surface inclusions on attenuating surface waves. The experiment was conducted in a thick deposit of silty clay soil. 5-m boreholes were

created in a 3 x 10 arrangement at the test site, as seen in *Figure 9*. A source excitation frequency of 50 Hz was used, and the wavelength of the signal was found to be comparable to the center-to-center borehole spacing, activating Bragg scattering. The results indicate up to a 2.3-times reduction in energy from the source. However, they also indicate a strong reflection of surface waves. In addition, the researchers found that a ring-type geometry, which would be needed protect a structure from all directions, engenders concentration effects in some scenarios. This could be detrimental to critical infrastructure [17].

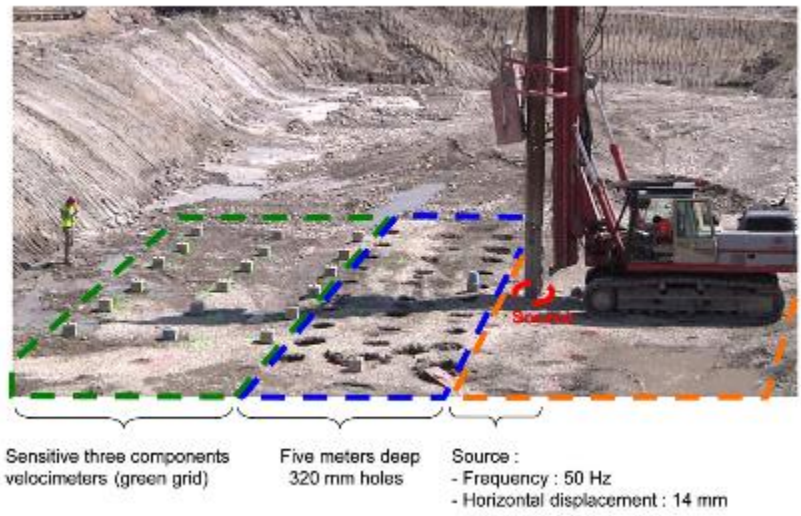

Figure 9 ***Borehole test setup. Source: Brule et al. (2014)***

Palermo et al. (2016) combined the findings from the metawedge designed by Colombi et al. (2016) and the information from studies on surface-embedded cylindrical inclusions to design a metabarrier. The metabarrier consists of periodic arrangement of rows and converts seismic waves into bulk waves that travel downward. After numerical verification of their design, Palermo et al. (2016) designed resonators consisting of a rigid aluminum tube, soft spring, and heavy steel mass, seen in *Figure 10*, to be tested experimentally. They embedded the resonators in polymer resin in a triangular lattice in order to achieve maximum density per lattice area. They found that band gap

formation does not rely on the arrangement, but that the resonance frequency can be tuned by varying the length of the resonators. The experiment was able to achieve low band gaps in the range of interest for civil engineering applications [18].

Figure 10 ***Resonators consisting of rigid aluminum tube, soft spring (aluminum bolt), and heavy steel mass. Source: Palermo et al. (2016)***

A numerical study by Miniaci et al. (2016) proposed the use of three-dimensional mechanical metamaterials, consisting of phononic crystals and locally resonant metamaterials, as a passive isolation strategy for seismic waves. They compared the effectiveness of boreholes, hollow metal cylinders, and locally resonant inclusions on the attenuation of bulk and surface waves, as seen in *Figure 11*. The study, which considers the effect of soil layers and viscoelastic damping, concluded that the hollow cylinder is most effective in attenuating seismic waves, and that a larger number of rows of cylinders has a more advantageous effect. Their results also demonstrate the existence of a very narrow band gap for locally resonant inclusions around their natural frequency. While the band gap is too small to effectively shield structures, they suggested experimenting with an array of inclusions to widen the band gap [19].

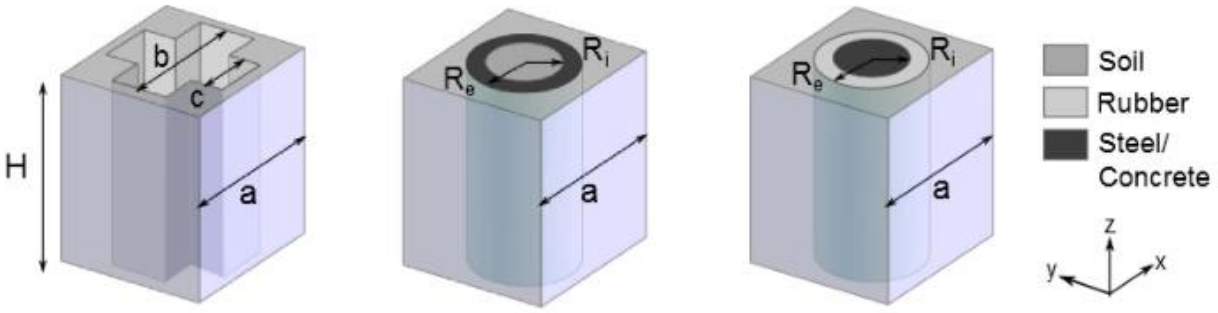

Figure 11 ***Unit cell of (left to right) borehole (cross-like cavity), hollow cylinder, and coated cylinder. Source: Miniaci et al. (2016)***

Mitchell et al. (2015) studied metaconcrete, or concrete containing bi-material spherical inclusions. These inclusions consist of a lead core with a rubber or nylon coating. They resonate at a certain frequency, and relative motion between the heavy metal core and surrounding mortar allows the inclusion to absorb energy. Mitchell et al. (2015) tested four different unit cell configurations, varying the radius of the core as well as the thickness and coating of the material in Abaqus to find eigenfrequencies. Then, they modeled arrays of aggregates within a mortar slab. One array consisted of 8 whole spherical inclusions and a second array consisted of 8 whole spherical inclusions plus an additional 28 quarter-spheres. The second array is shown in *Figure 12.* Each array was tested for each of the four configurations of the unit cell. A transmission coefficient, plotted against forcing frequency, was used to analyze the effect of the aggregates in the slab on propagating waves. In *Figure 13* and *Figure 14*, dips in the transmission coefficient can be observed near, but not exactly at, the resonant frequencies of the inclusions. They suggest Bragg scattering or numerical interference may have affected the results. Mitchell et al. concluded that the inclusions with the stiffer nylon coating performed better than those with the rubber coating. In addition, more inclusions resulted in a greater reduction in transmission and wider frequency range of influence [20]. While this study is one of the few that involves the performance of metamaterials for bulk

waves, it lacks experimental validation and does not attempt to widen the range of frequencies in which a dip in transmission coefficient is observed.

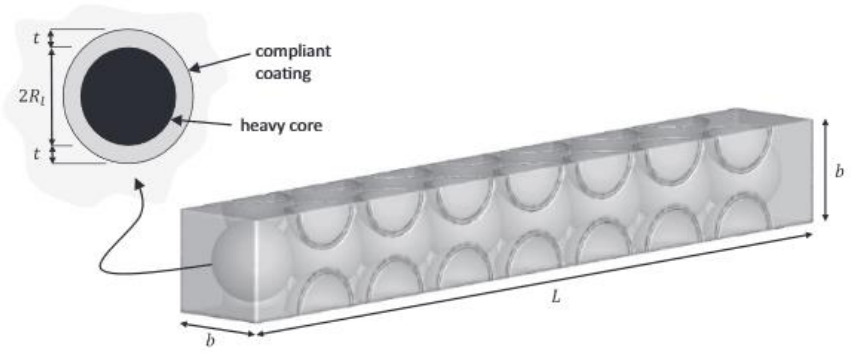

Figure 12 ***Metaconcrete slab showing inclusion structure. Source: Mitchell et al. (2015)***

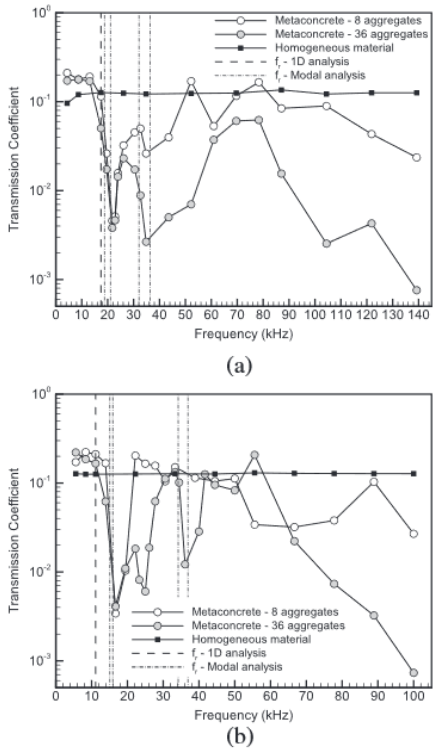

Figure 13 ***Transmission coefficient versus frequency for metaconcrete slab consisting of (a) 1mm, (b) 3mm nylon-coated aggregates. Source: Mitchell et al. (2015)***

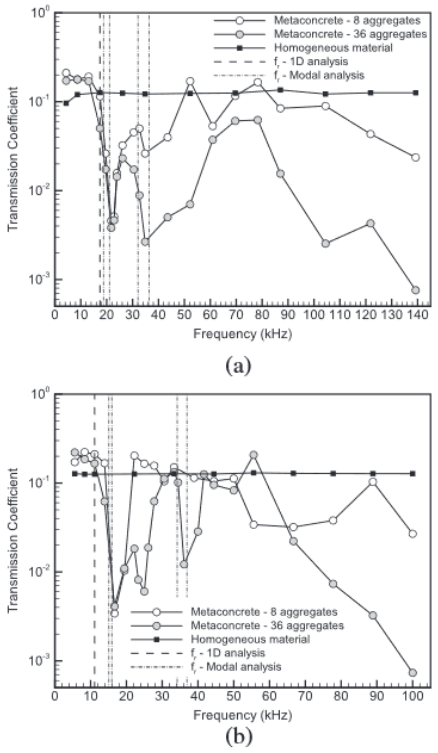

Figure 14 ***Transmission coefficient versus frequency for metaconcrete slab consisting of (a) 1mm, (b) 3 mm rubber-coated aggregates. Source: Mitchell et al. (2015)***

Krodel et al. (2015) conducted one of the most applicable studies to this thesis to date. They designed an array of cylindrical tubes, each containing a heavy steel mass suspended by soft bearings designed to possess a different eigenfrequency of 4 to 7 Hz. This effectively created what they referred to as a "rainbow trap," splitting propagating surface waves into a spatial spectrum by varying the bearing stiffness. Results from the numerical study demonstrated that changes in ordering and spacing of the resonators did not affect the transmission spectrum, but that a greater number of resonators correlated directly to an increase in the wave attenuation. Next, Krodel et al. built a 1:30 scaled experimental setup to verify their concept. Resonators were placed from lowest to highest resonant frequency in a box of sand, which is assumed to be a non-dispersive material. Longitudinal and shear waves were excited on one side of the box using an electromagnetic shaker and transmission was measured on the other end using an accelerometer. For a total of 15 resonators designed to have an eigenfrequency range of 134 to 208 Hz (real-scale range of 4.46 to 6.93 Hz), a maximum attenuation of -11.7 dB was achieved. The design of the experimental resonators as well as a visualization of the “rainbow trap” is shown *Figure 15.* Krodel et al. was able to match numerical results experimentally and widen the band gap of resonators at the desired seismic range. However, they could not measure the energy propagating in the experiment and expect that some reflection occurred [21].

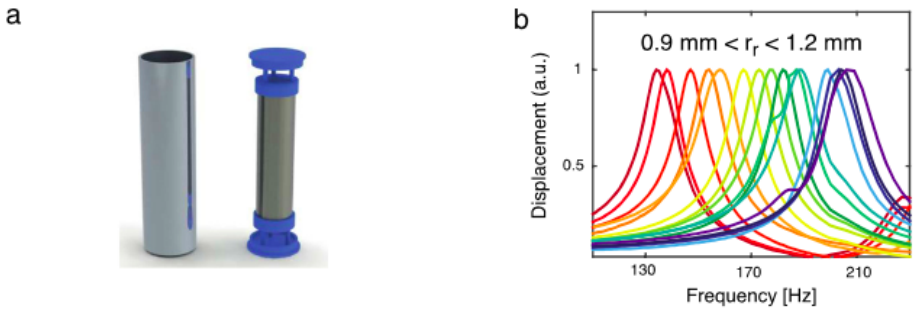

Figure 15 ***Experimental study of “rainbow trap”. (a) Experimental resonators consisting of outer aluminum tube containing steel rod, and connected polymeric springs, (b) Resonant frequencies of 15 resonators with variable spring stiffness, creating a “rainbow trap.” Source: Krodel et al. (2015)***

Research Objectives

Although the completed investigations show essential and promising development in the use of metamaterials as seismic and vibratory wave attenuators, many knowledge gaps still exist in this field of research. For example, minimal physical experiments have been conducted to confirm observed simulation results. In addition, there is a decent understanding of the ability of resonator-based metamaterials to produce a band gap at their resonant frequency. However, for practical applications, the ability to produce a wide band gap at low frequencies (<50 Hz) is desirable for seismic applications.

The objective of this research is to address some of the knowledge gaps in this research area by focusing on designing resonators that perform at a low frequency and could be adapted in a physical experiment to study the attenuation of a bulk wave in a half-space. The main objectives are:

1. To conduct a sensitivity analysis on bi-material spherical resonators to inform design of new improved resonators
2. To find a size and arrangement of inclusions that increases the band gap
3. To create embedded resonators capable of attenuating vertically propagating bulk waves

Chapter 2

Metaconcrete Modeling

Analysis of Unit Cell

The first research task revolved around the re-creation and testing of the metaconcrete slab designed by Mitchell et al. (2015) [20]. The model and results from the paper serve as a foundation for the design and testing of new improved resonators.

Geometry and Boundary Conditions

As in Mitchell et al (2015), four configurations of a unit cell were tested. The 0.3-m square unit cell consisted of a heavy spherical core and elastic coating, encompassed in a block of mortar. The corresponding geometrical and material details are shown in *Table 1*, where R_t is the radius of the lead core and t is the thickness of the coating. The testing of different configurations allows for an analysis of the influence of core size, coating thickness, and coating material on the eigenfrequencies of the resonator.

Table 1 ***Geometry and material of unit cell configurations. Source: Mitchell et al. (2015)***

Configuration	R_l (mm)	t (mm)	Coating
1	11	1	Nylon
2	9	3	Nylon
3	11	1	Rubber
4	9	3	Rubber

The unit cell was created using COMSOL Multiphysics [22] and is shown in *Figure 16*. The material parameters from Mitchell et al, summarized in *Table 2*, were used. The mortar cube is 0.3 m on all sides, and the dimensions are consistent for the four configurations.

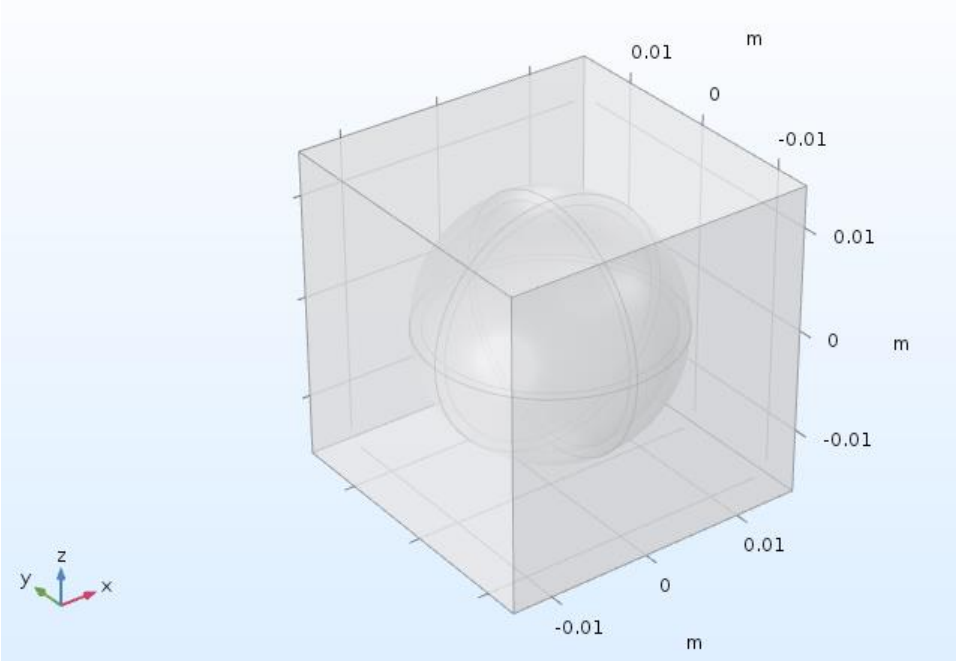

Figure 16 ***The COMSOL model of the unit cell containing bi-material spherical inclusion.***

Table 2 ***Material parameters of resonators. Source: Mitchell et al. (2015)***

Material	ρ (kg/m^3)	E (GPa)	ν
Mortar	2500	30	0.20
Lead	11,400	16	0.44
Nylon	1150	1.0	0.40
Rubber	900	0.01	0.49

A user-controlled adaptive mesh was used, ensuring that the maximum element size was less than one-tenth of the wavelength of a P-wave in mortar. A mesh size convergence was performed, and

a portion of this analysis is seen in *Figure 17*. A maximum element size (MES) of 0.004 m and corresponding mesh size was determined as adequate.

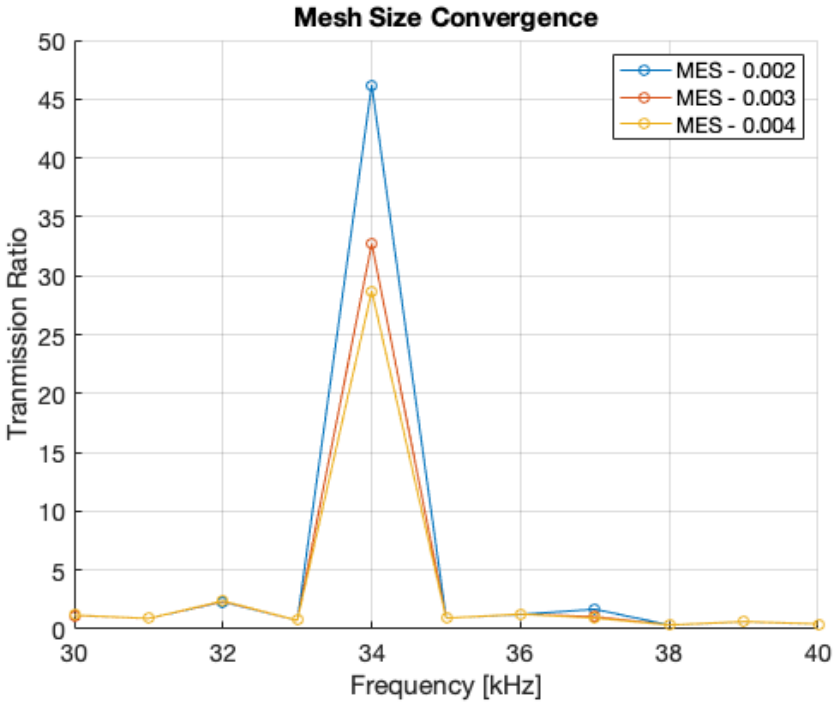

Figure 17 ***Mesh size convergence comparing Maximum Element Size (MES).***

Eigenfrequency Analysis

While Mitchell et al. (2015) refers to the geometry as a periodic unit cell, analysis showed that periodic boundary conditions were not applied in the determination of the eigenfrequencies corresponding to each configuration, which are shown in *Table 3*. Instead, fixed constraint boundary conditions, in which $u_x = u_y = u_z = 0$, were applied to all faces of the cube in order to match the results.

The mode shape analysis was consistent with what is reported in Mitchell et al. (2015). The first mode shape represents rigid body rotation of the core. The second mode shape, the one of most

interest in this study, is rigid body translation of the core as it oscillates in the coating material. The second mode shape for Configuration 1 is shown in *Figure 18*. The third and fourth mode shapes represent vibration and bending of the core and/or coating.

Table 3 ***Modal eigenfrequencies for each configuration. Source: Mitchell et al. (2015)***

Configuration	Eq. (1) (kHz)	Finite element unit cell (kHz)			
		Mode 1	Mode 2	Mode 3	Mode 4
1	17.41	18.84	21.12	32.14	36.42
2	11.11	15.08	15.94	34.19	36.92
3	1.74	1.99	5.99	25.00	27.70
4	1.11	1.51	3.39	10.44	11.12

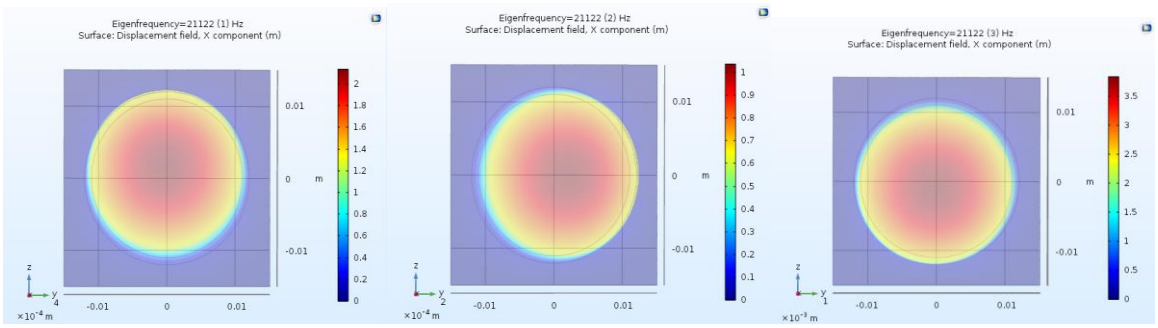

Figure 18 ***Second mode eigenfrequency for configuration one, achieved in COMSOL Analysis.***

Metaconcrete Slab

A metaconcrete slab mimicking the one in Mitchell et al. was built in COMSOL Multiphysics [22]. First, a mortar slab of dimensions L x b x b was created with L = 0.24 m and b = 0.03 m. A periodic arrangement of the resonators was added to the slab, spaced at 0.03m centers. Another arrangement, including the addition of 28 quarter spheres around the edges of the mortar slab, was also created. Therefore, two metaconcrete slabs were created: one with a total of 8 whole bi-material spherical

inclusions, or embedded resonators, and one with a total of 36 inclusions. The slabs are shown in *Figure 19*.

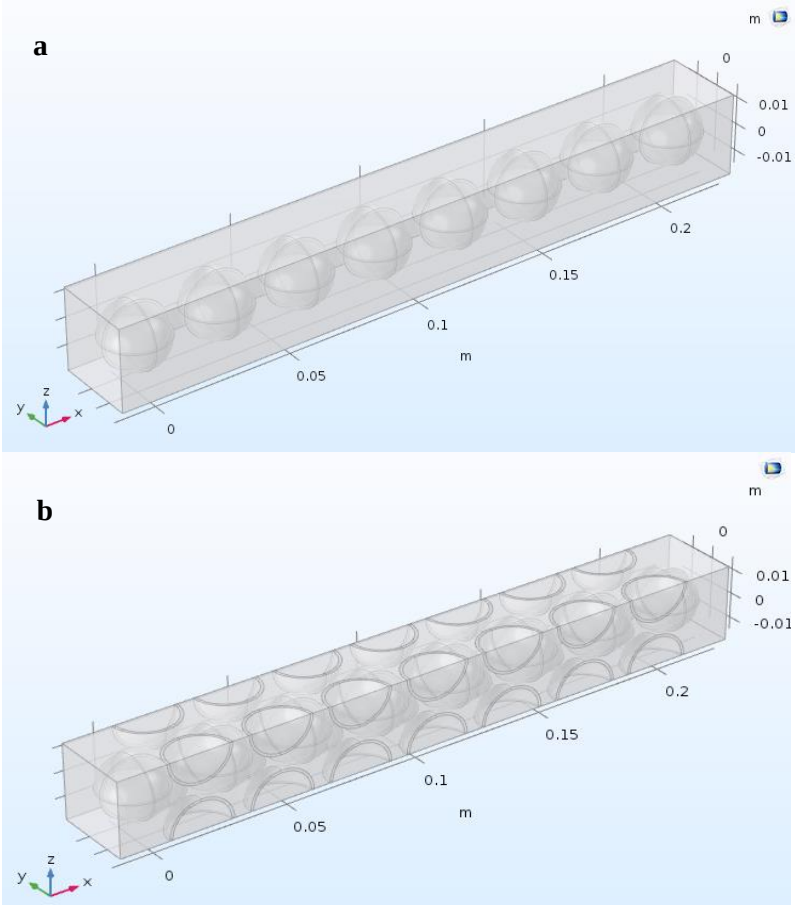

Figure 19 ***Metaconcrete slab with (a) 8 whole inclusions, (b) 8 whole inclusions and 28 quarter spheres (36 total inclusions).***

Simulation of Wave Propagation in the Frequency Domain

In Mitchell et al (2015), a time domain analysis in Abaqus [23] was used to analyze the slab behavior in attenuating waves. However, due to the large computing time required for time domain analysis in COMSOL Multiphysics, a frequency domain analysis was instead used. A prescribed displacement was applied to the end face of the slab in x-direction. A traction-free boundary

condition was applied to the other end face, and periodic boundary conditions were applied to the lateral faces of the lab.

An analysis of each configuration at the second mode of the unit cell was performed to confirm that resonance occurs at the expected frequencies. For each configuration, a section view was created to view displacement along the length of the slab. In addition, a line graph was plotted showing total displacement vs. length along the resonator (arc length). These views are shown for each configuration in *Figure 20* and *Figure 21*. The results confirm that resonance of the inclusions occurs and the displacement that the slab experiences decreases as the distance from the source increases.

a

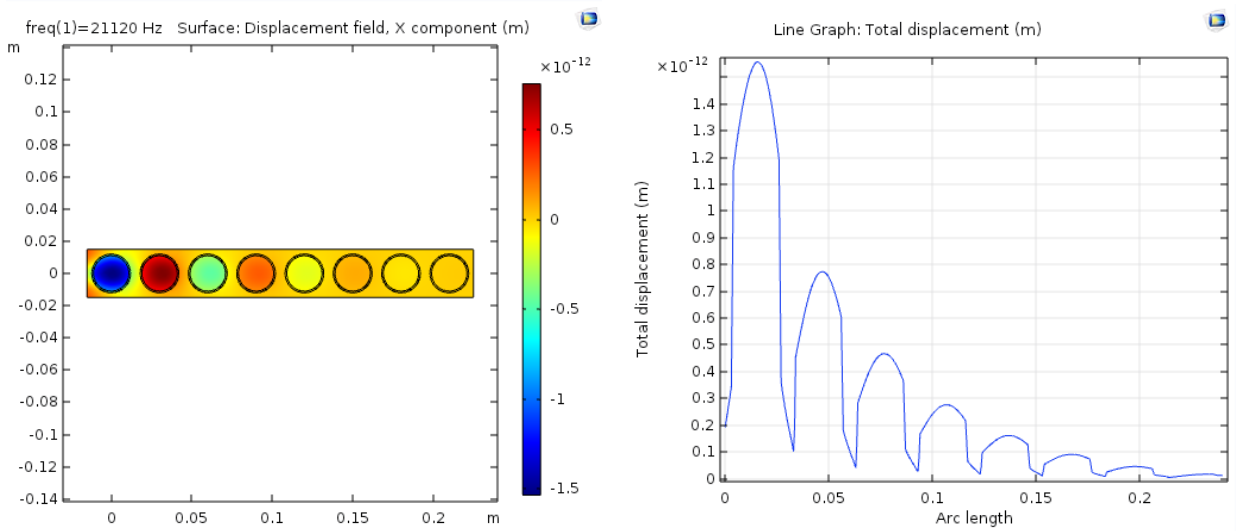

b

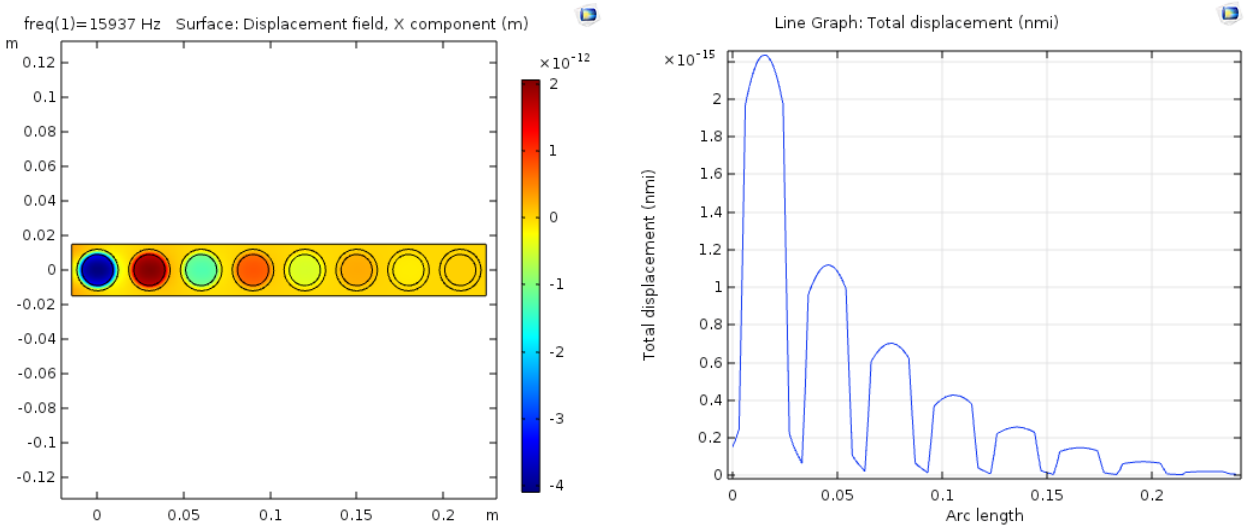

Figure 20 ***Section view of displacement and line graph of displacement vs. length along slab for nylon-coated resonators, (a) Configuration 1, (b) Configuration 2.***

a

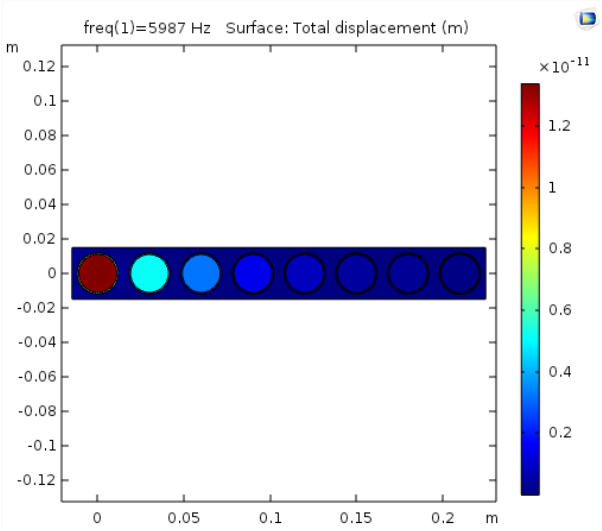

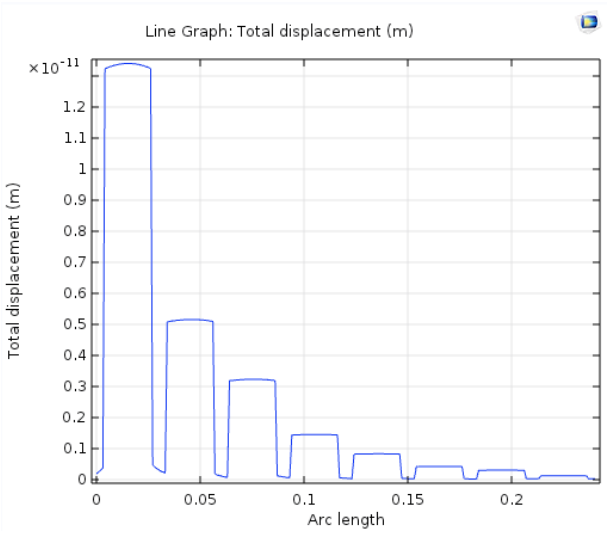

b

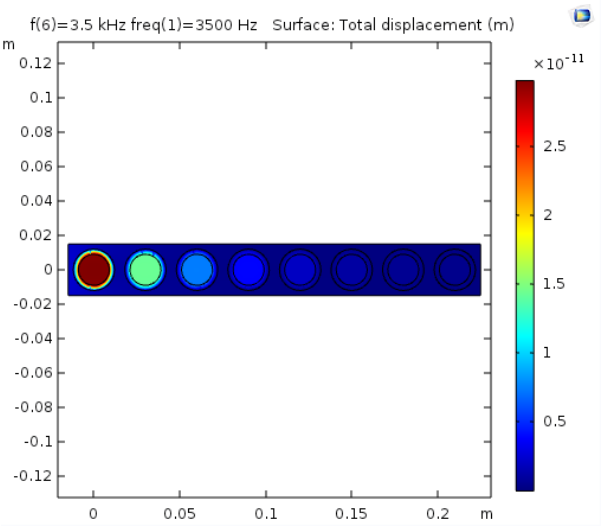

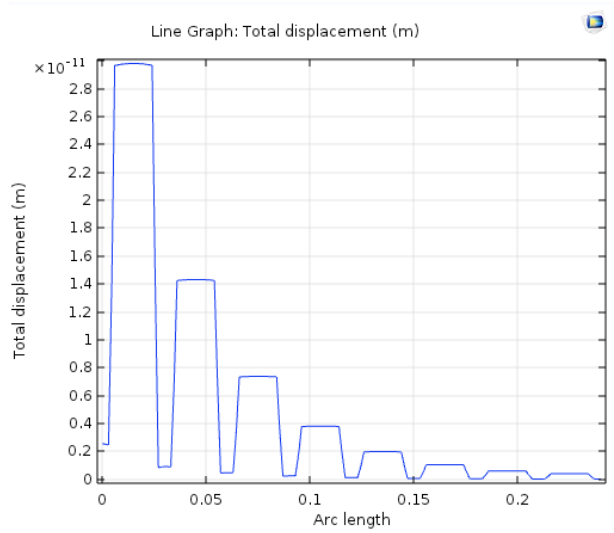

Figure 21 ***Section view of displacement and line graph of displacement vs. length along slab for rubber-coated resonators,*** (a) Configuration 3, (b) Configuration 4.

Next, a parametric sweep over frequency was added to the study. A quantitative method was needed to compare the transmission of displacement along the slab when analyzed at different frequencies. The Transmission Ratio was defined and calculated as the displacement at the center of the free face divided by the displacement at the center of the face that the prescribed displacement was applied on. This value was then plotted vs. frequency. A band gap was defined to exist at frequencies where the Transmission Ratio is less than 1. The results are shown in *Figure 22* and *Figure 23*.

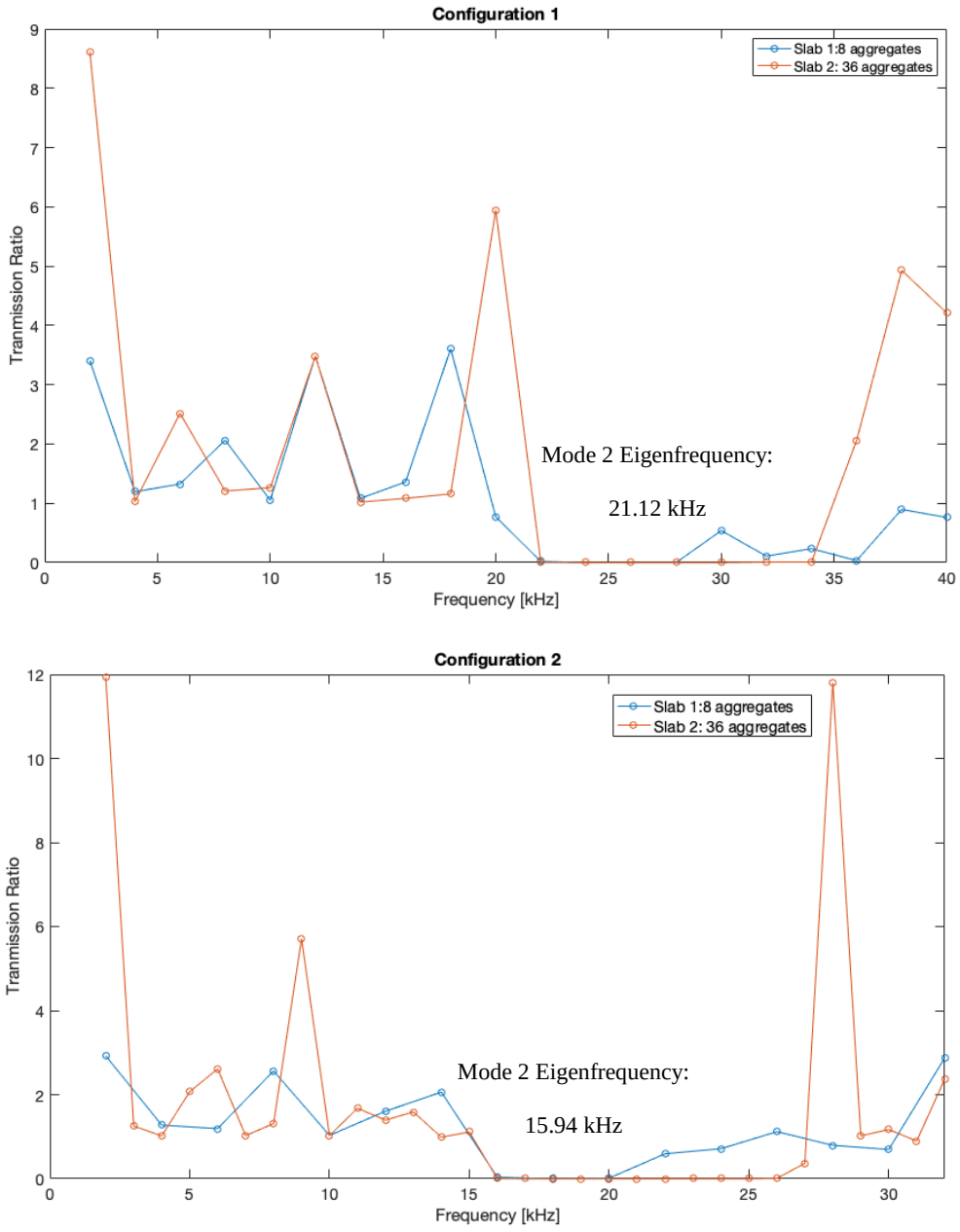

Figure 22 ***Plot of Transmission Ratio vs. frequency for nylon-coated resonators.***

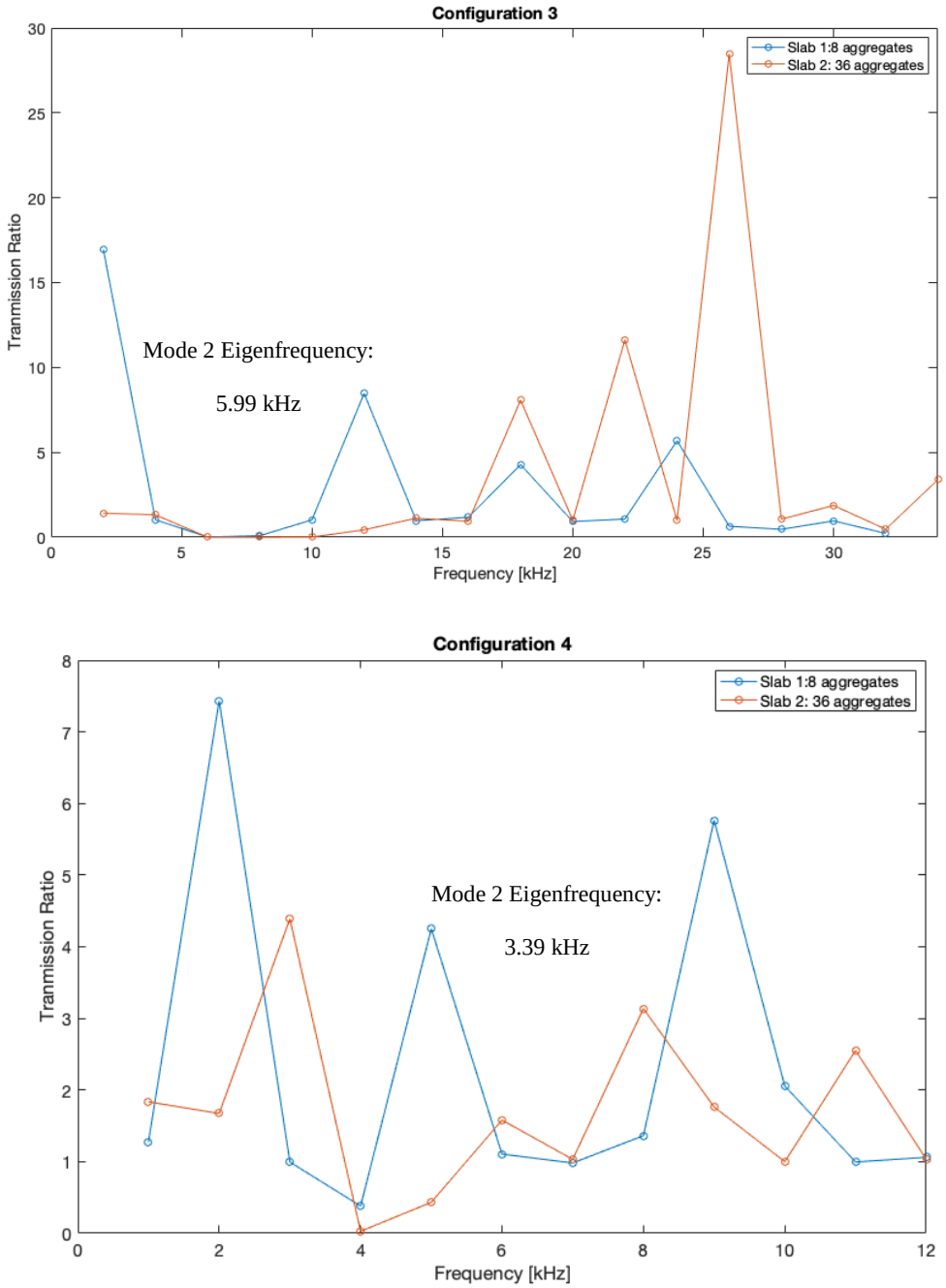

Figure 23 ***Plot of Transmission Ratio vs. frequency for rubber-coated resonators.***

Although Mitchell et al. (2015) calculated the transmission coefficient differently, the results achieved in this study are comparable to those achieved in the paper. A dip in transmission is found

near the corresponding mode 2 eigenfrequency. For most configurations, the more densely-packed 36-inclusion slab demonstrates a wider band gap than the 8-inclusion slab. In addition, the dip in transmission coefficient is larger and more consistent for the stiffer nylon-coated resonators than that for the rubber-coated resonators.

Large jumps in the transmission ratio are observed at certain frequencies, such as at 28 kHz in Configuration 2. An investigation was conducted to determine if these points were anomalies caused by low resolution of the frequency axis. *Figure 24* shows that the jump is not an anomaly, as there are data points leading up to it. To further analyze the wave transmission along the metaslab at the different frequencies, a section view of the displacement along the length of the slab was observed, as well as a line graph of the data. In *Figure 25*, the section view and line graph are shown for Configuration 2 at 26 kHz, where the Transmission Ratio is near zero, as compared to the section view and line graph for Configuration 2 at 28 kHz, where the Transmission Ratio has a high value. The displacement gradually decreases at 26 kHz along the length of the slab. However, at 28 kHz the line graph and section view show that there is no pattern for the value of displacement along the slab length. These results suggest that the large jumps in Transmission Ratio could be due to resonance of the metaconcrete slab at certain frequencies.

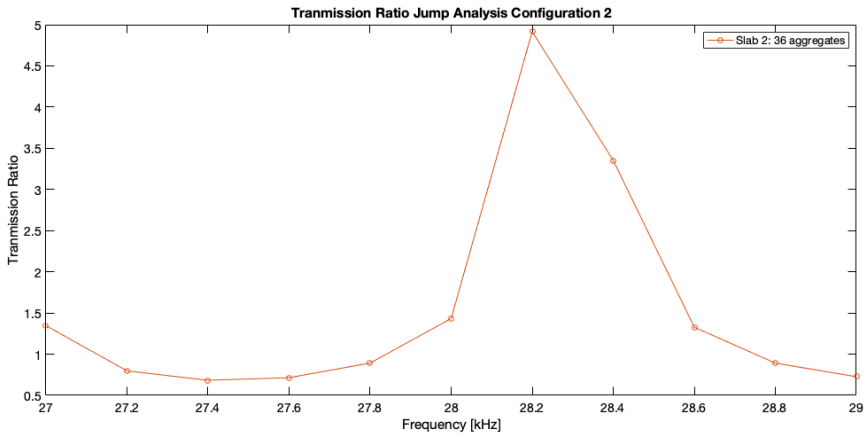

Figure 24 ***Analysis of jump in Transmission Ratio.***

a

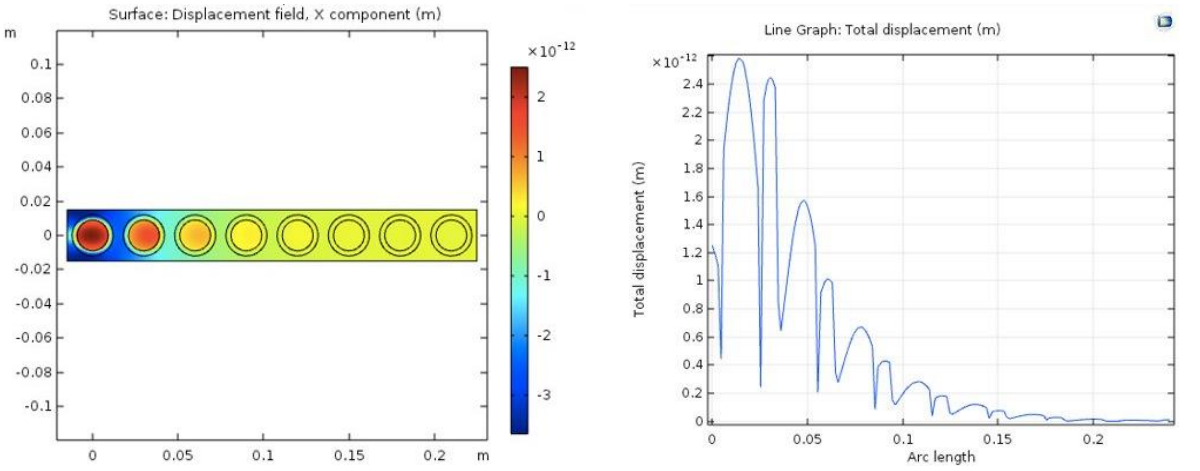

b

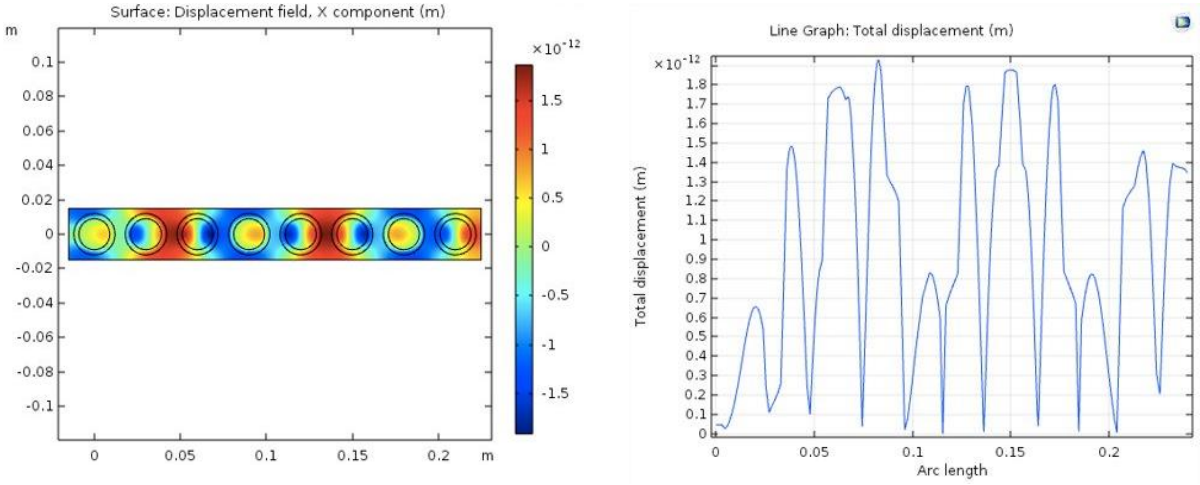

Figure 25 ***Section view of displacement and line graph of displacement vs. length along slab for Configuration 2, Slab 2: 36 aggregates at (a) 26 kHz, (b) 28 kHz.***

Sensitivity Analysis

A detailed sensitivity analysis was needed to analyze how changing the geometry and material properties affects the transmission ratio in order to inform design of the improved resonators. In Mitchell et al, the expected natural frequency value, *f*, of the resonator is calculated by

$$f = \frac{1}{2\pi}\sqrt{\frac{3}{2}\frac{E_c}{R_t t \rho_t}} \tag{1}$$

where E_c is the Young's modulus of the coating, R_t is the radius of the core, t is the thickness of the coating, and ρ_t is the density of the core. It was determined that this formula is satisfactory in estimating the frequency at which the transmission of the slab should be analyzed. However, the paper only provided an investigation of two different E_c values. In addition, it did not provide simulation results for varying the thickness of the coating, *t*.

Therefore, a sensitivity analysis was undertaken to determine how the band width could be shifted or widened for a different natural frequency achieved by varying the thickness of the coating, the Young's modulus and density of the coating, and the density of the core.

Four different coating thicknesses were tested on the 36-inclusion slab: 1.5 mm, 2 mm, 2.5 mm and 3 mm. The results agree with Equation 1, showing that a higher thickness results in a lower resonant frequency. As seen in *Figure 26*, the width of the band gap is not affected by the coating thickness, remaining consistent at approximately 7 kHz. However, the band gap is consistently shifted to a lower frequency range for a higher coating thickness.

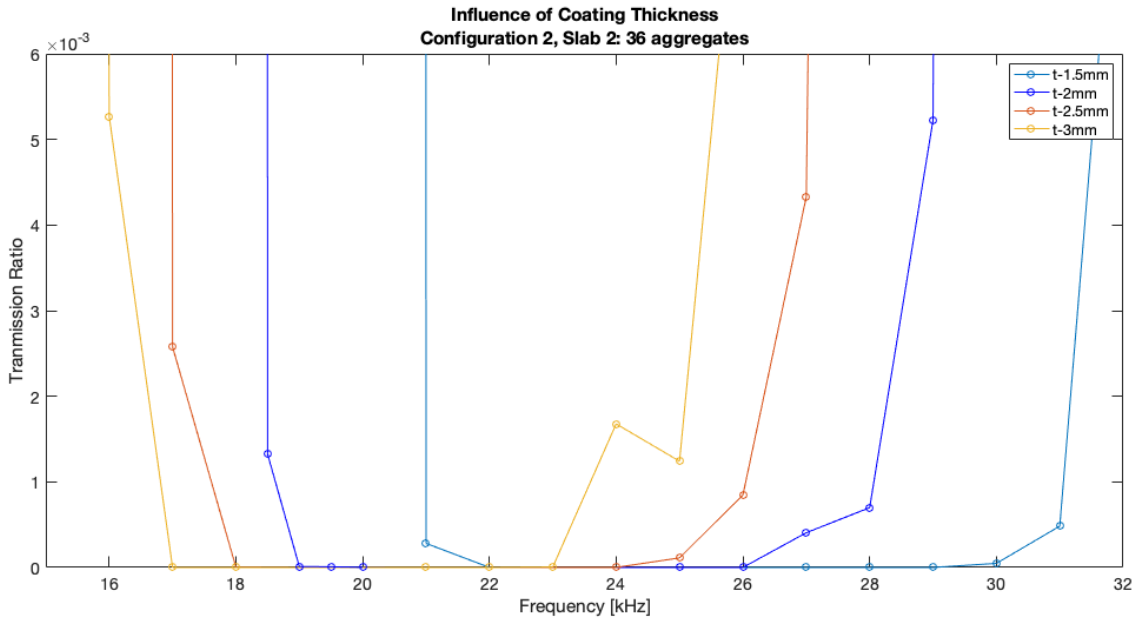

Figure 26 ***Effect of varying coating thickness.***

Next, six different coating materials were analyzed. Each trial had a different combination of density and Young's modulus values, corresponding to practical rubber-like material parameters, as shown in *Table 4.* According to Equation 1, only the Young's modulus of the coating affects the natural frequency of the resonators, not the density of the coating. Therefore, for the six trials, there are four corresponding natural frequencies. The results are shown in *Figure 27*.

Table 4 ***Coating materials analyzed.***

	Density (kg/m^3)	Young's Modulus (GPa)	Natural Frequency (kHz)
Rubber	900	0.01	1.11
Rubber - II	1150	0.01	1.11
Silicone	1500	0.05	2.48
Nylon	1150	1	11.11
Nylon - II	1000	1	11.11
PET Plastic	1300	2	15.71

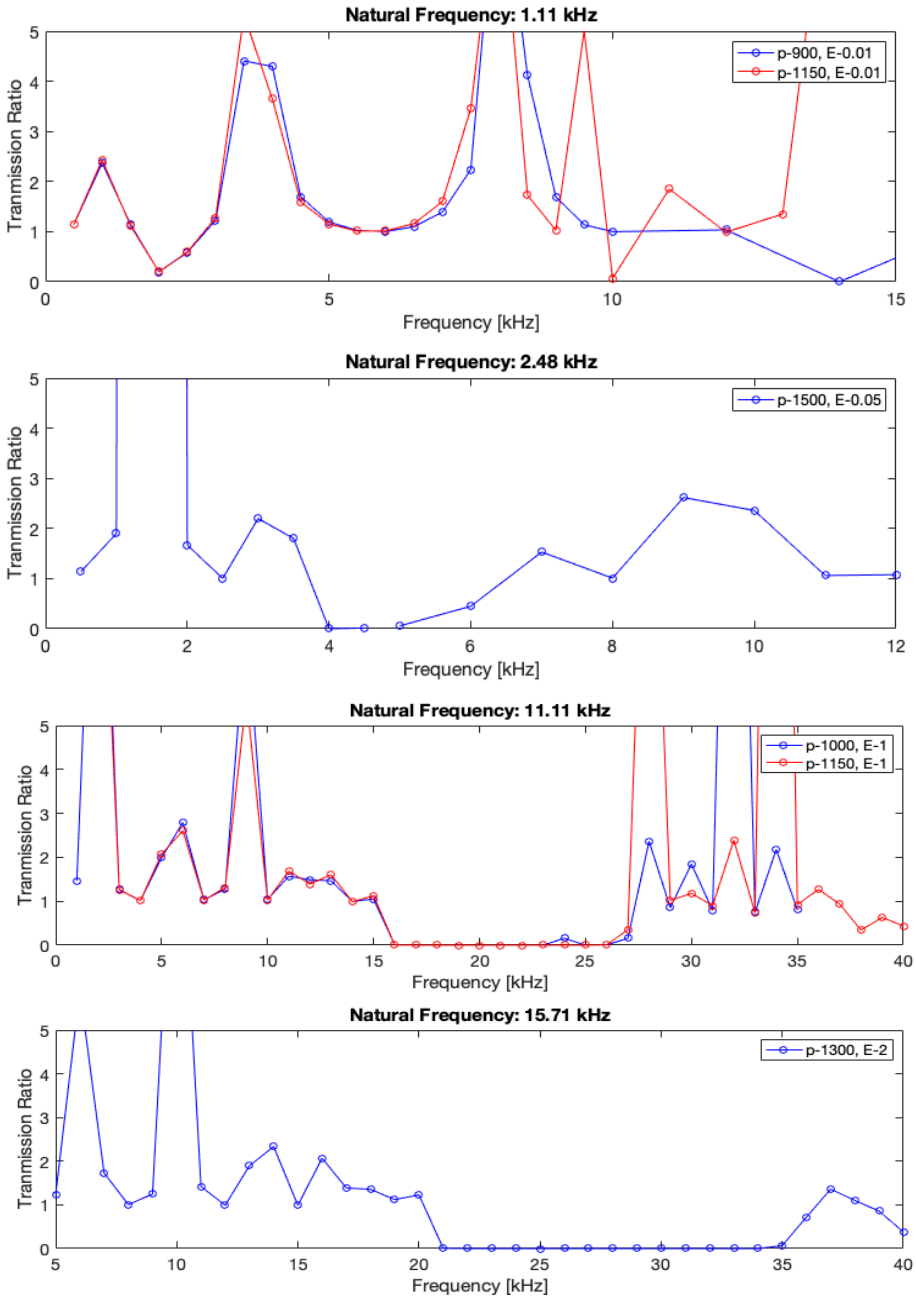

Figure 27 ***Effect of coating material on band gap.***

For a given Young's modulus of the coating material, varying the density does not significantly change the band gap. However, the higher the Young's modulus, the higher the natural frequency,

which agrees with Equation 1, and the higher frequency-range band gap. In addition, a higher Young's modulus results in a wider band gap.

Three different core materials were analyzed next. The original core, lead, has a very high density, which is ideal in producing a low resonant frequency. However, lead is toxic to humans, so it is not practical for experimental use. It is difficult to find a material that is widely available, inexpensive, and practical to use as a construction material, while still maintaining the high density of lead. Two metals – steel and brass – were found to be the closest match to the criteria. The material properties of the three core materials tested are summarized in *Table 5*. The simulation results are shown in *Figure 28*.

Table 5 ***Material properties of different core materials.***

	Density (kg/m^3)	Young's Modulus (GPa)	Poisson's Ratio
Lead	11400	16	0.44
Brass	8500	100	0.31
Steel	7800	200	0.26

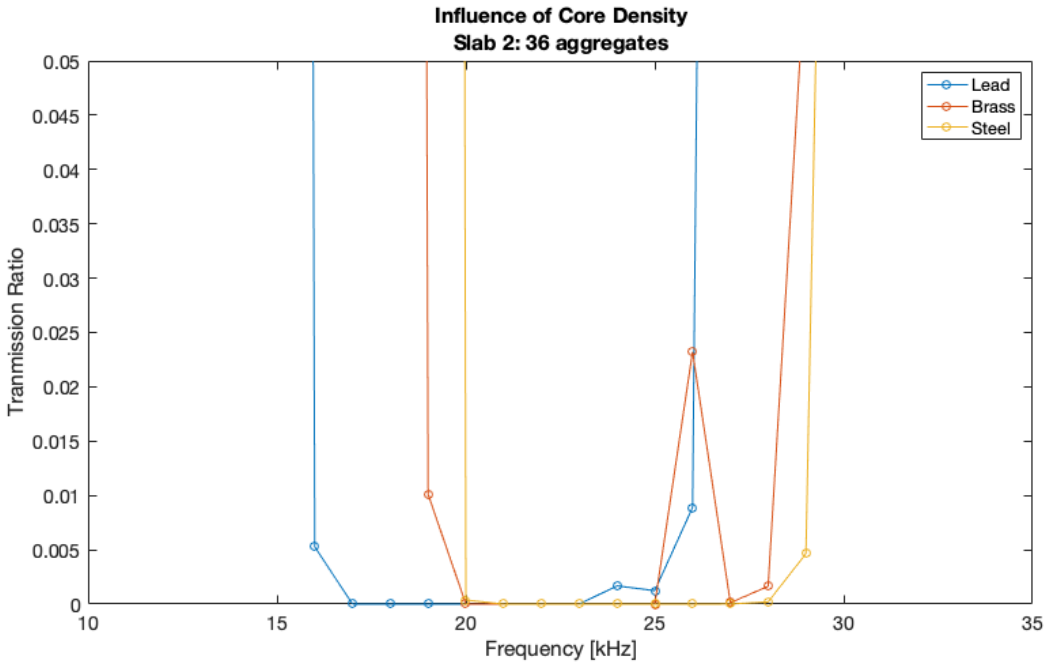

Figure 28 ***Effect of core density on band gap.***

As expected, the higher density of lead creates a resonant frequency and subsequent band gap at lower frequencies. However, the band gap does not shift significantly for the lower-density core materials of brass and steel. Therefore, these can be viable core materials for alternate resonators.

In summation, the sensitivity analysis demonstrates that for the purpose of achieving a wide and low-frequency band gap, a stiffer coating material, thicker coating, and denser core are desired. As all of these findings are in agreement with Equation 1, it is accepted as a good estimation of the resonant frequency of the bi-material spherical inclusions.

Shear Boundary Load

While the demonstrated ability of the metaconcrete resonators to produce band gaps when a vertically propagating bulk wave is applied to the end face of the slab is promising, there are many other types of earthquake waves. Shear waves, which travel perpendicular to the direction of propagation, cause more damage to structures than P-waves do during earthquakes. Therefore, analysis of the transmission through the metaconcrete slab subjected to a shearing boundary load is conducted to determine if the resonators can successfully function in this application.

All four configurations are tested with a prescribed displacement applied to the end face of the slab in the z-direction. The other boundary conditions remained the same as in previous testing. The resulting Transmission Ratio was calculated at each frequency and plotted. *Figure 29* and *Figure 30* show the results of the shear study, as compared to the normal case of a boundary load applied in the x-direction. For configuration 2, the 3D deformation of the slab subjected to a shearing frequency within the band gap, and a shearing frequency outside of the band gap, is plotted. *Figure 31* clearly shows that resonance is occurring at frequencies within the band gap.

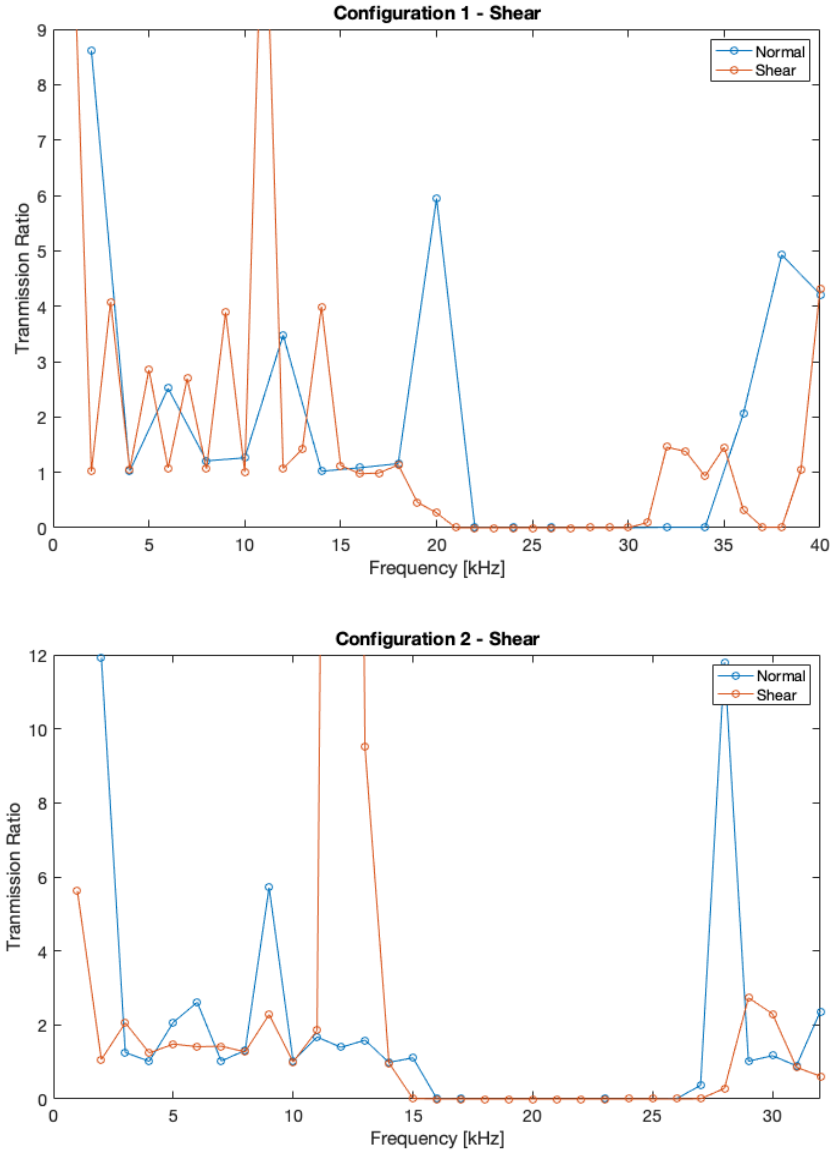

Figure 29 ***Plot of Transmission Ratio vs. frequency for nylon-coated resonators subjected to shearing deformation.***

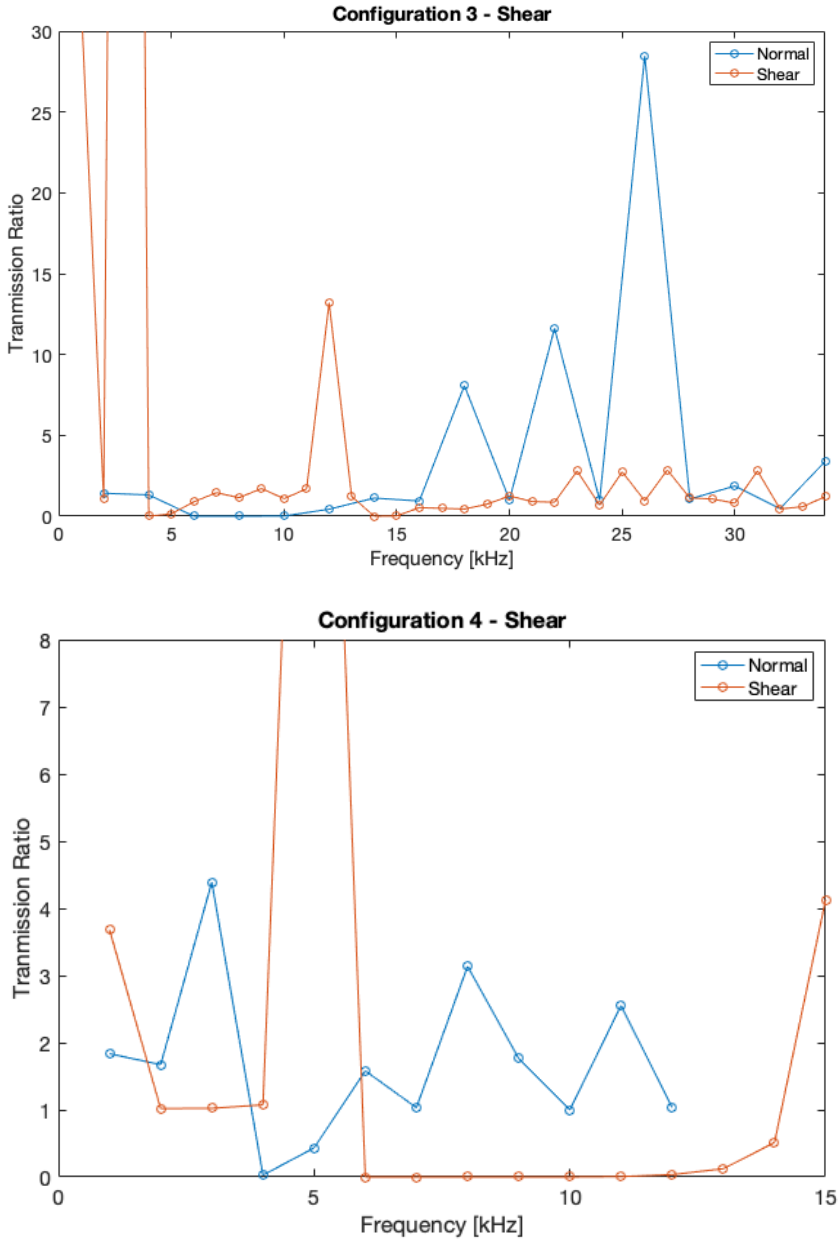

Figure 30 ***Plot of Transmission Ratio vs. frequency for rubber-coated resonators subjected to shearing deformation.***

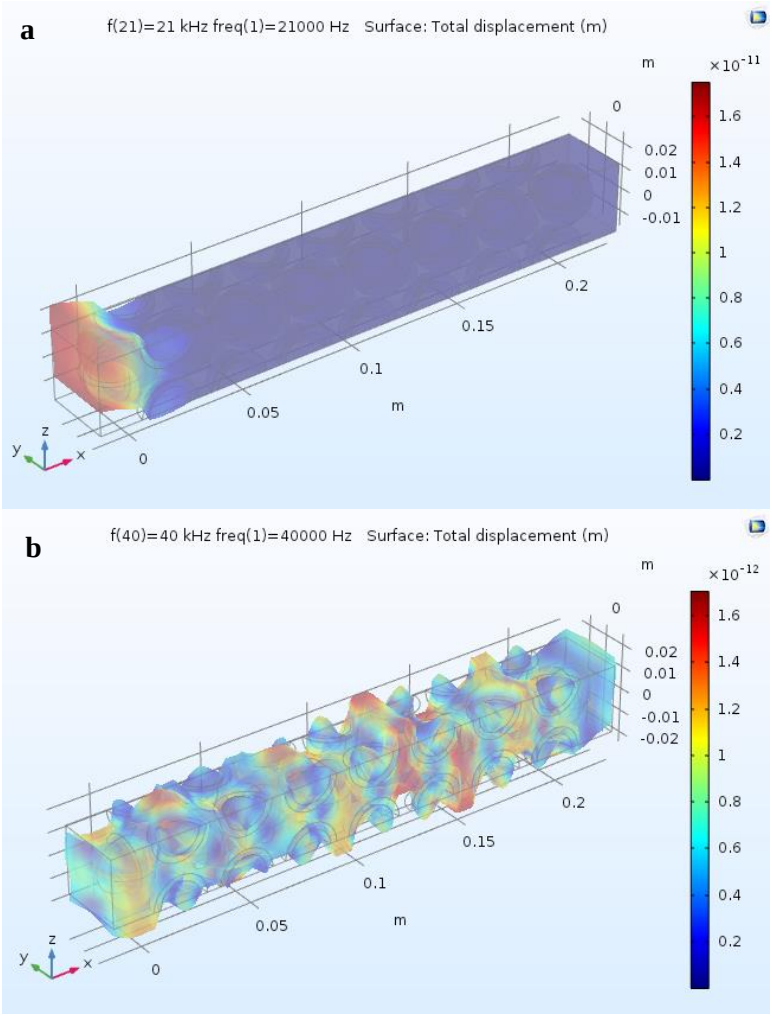

Figure 31 ***Plot of 3D displacement for shearing case (a) within band gap frequency, (b) outside of band gap frequency.***

A band gap is present near the P-wave values for the shear case in all four configurations. In configuration 1, the band gap is approximately the same width but shifted to a lower frequency range. For configuration 2, the band gap has the same center value, but is approximately 1 kHz wider on both the low and high end of the band gap. For configuration 3, two band gaps are present. One occurs before the P-wave bandgap and the second occurs after it. The one that occurs after is more pronounced, and approximately the same width as the P-wave bandgap. Overall, the

transmission is lower in this configuration for the shearing load. For configuration 4, the band gap is much wider, but at a higher frequency range. *Figure 32* summarizes these results.

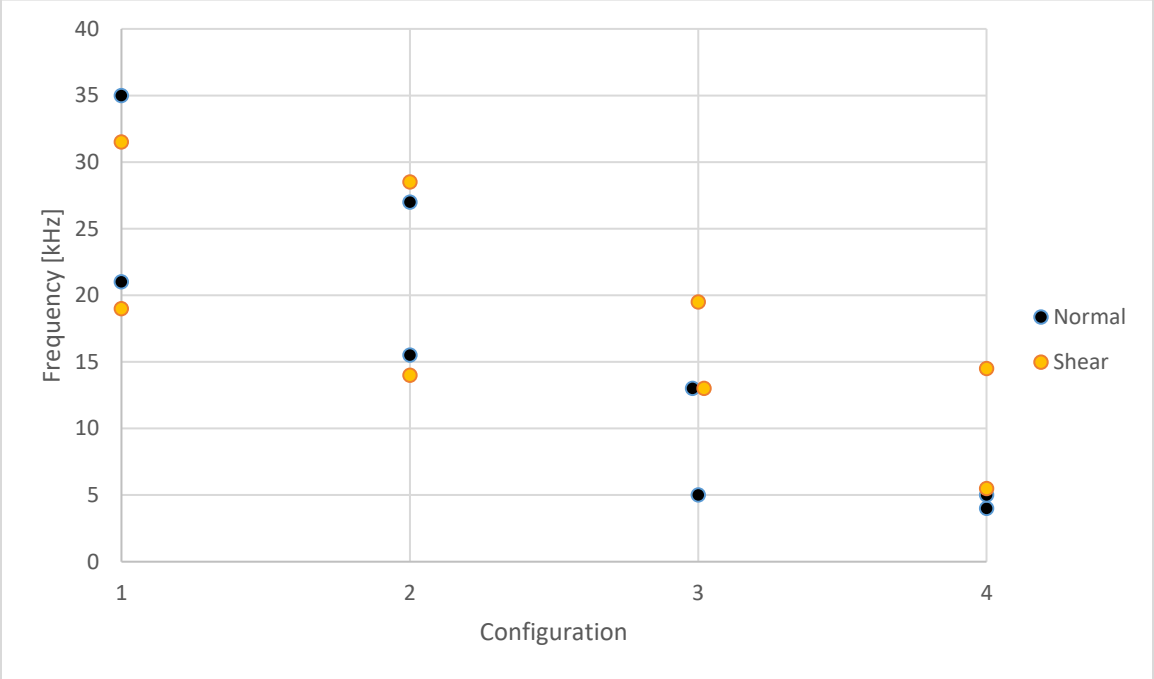

Figure 32 ***Band gap comparison for shearing load***

The results show that the band gap's frequency range is not consistently increased/decreased nor widened/narrowed when applying a shearing load rather than a compressing load. However, the fact that a band gap is produced for all four configurations under a shear load is an important development. Additional work is necessary to determine the influences of the band gap when subjected to a shearing boundary load.

Investigation of Graded Resonator Array

Krodel et al. (2015)'s "rainbow trap" is one of only a few attempts to widen the band gap produced by a graded array of resonators. They found that varying stiffness between individual resonators widened the band gap, but that changes in ordering and spacing of the resonators did not affect the transmission spectrum [21]. Their successful results inspire further investigation into this concept.

The nylon-coated resonators in configuration 1 and configuration 2 for the 36-aggregate slab provided the most distinct band gaps, both in compression and shear loading. Therefore, a metaconcrete slab consisting of a graded array of these configurations is modeled. The first four center aggregates and first four series of quarter-inclusions have a 3 mm nylon coating (configuration 1). The next four center aggregates and next three series of quarter inclusions have a 1 mm nylon coating (configuration 2). The geometry of the slab is demonstrated in *Figure 33*.

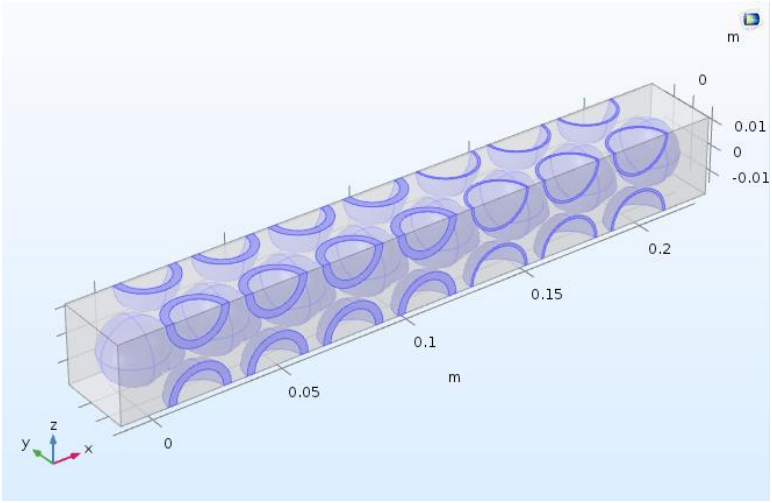

Figure 33 ***Geometry of graded metaconcrete slab.***

Then, a shearing load is applied to the end face of the slab in the z-direction and the transmission spectrum is plotted. The results are shown in *Figure 34*.

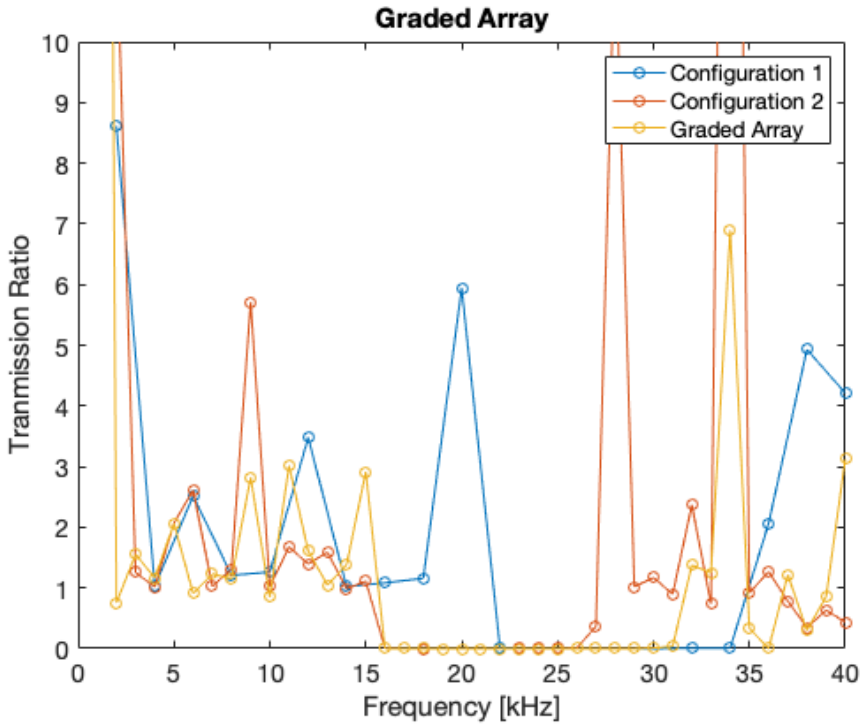

Figure 34 ***Plot of Transmission Ratio vs. frequency for graded metaconcrete slab.***

The results demonstrate a wider band gap for the graded array of resonators than both the configuration 1 and configuration 2 case. The ability to design for a wide range of resonant frequencies is invaluable in the concept of creating a seismic shield. With more testing, the optimum stiffness variation of the resonators could widen the band gap to an even larger frequency range. Ultimately, using resonators designed to have an eigenfrequency within seismic range, the ability to reduce transmission over the frequency spectrum of seismic waves is entirely possible based on these results.

Soil Simulations

Until this point, the simulations have taken place using a mortar block. Mortar is modeled as a homogeneous linear elastic material. For the purpose of earthquake mitigation, the resonators would most likely be placed in soil, which is a much more complex material than mortar. Therefore, performing simulations in soil is necessary.

As a transitional step, the tests were repeated in COMSOL Multiphysics [22] using parameters for soil, but still assigning it as a linear elastic material. Medium dense, dry, uniform sand was chosen as the type of soil because it exhibits the most linear behavior in reality. The parameters used for the sand are shown in *Table 6*, and the results are shown in *Figure 35* and *Figure 36* [24], [25].

Table 6 ***Material properties used for linear elastic soil analysis.***

	Density (kg/m^3)	Young's Modulus (GPa)	Poisson's Ratio
Medium Dense, Dry, Uniform Sand	1600	0.04	0.32

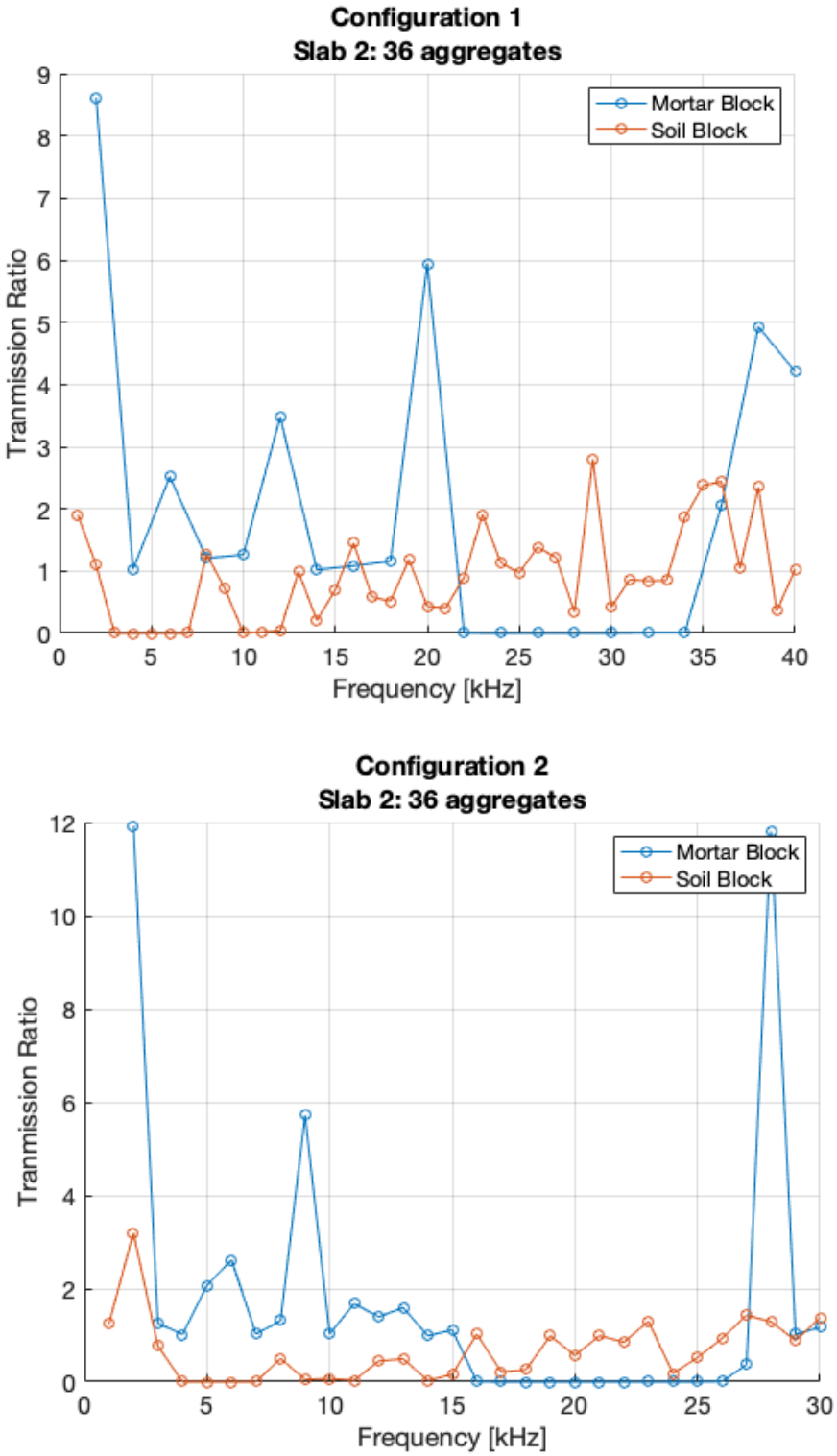

Figure 35 ***Plot of Transmission Ratio vs. Frequency for nylon-coated resonators embedded in mortar and soil.***

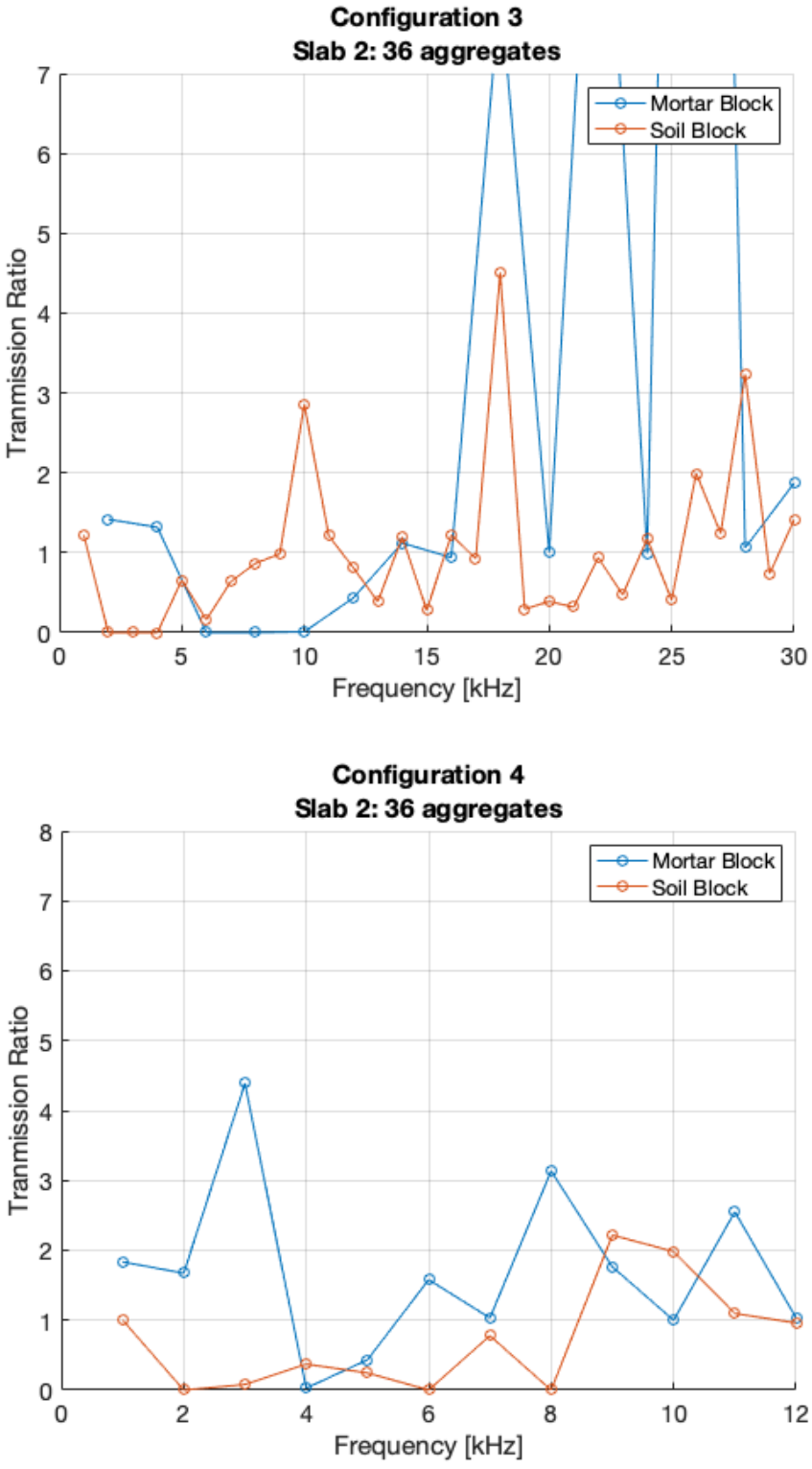

Figure 36 ***Plot of Transmission Ratio vs. Frequency for rubber-coated resonators embedded in mortar and soil.***

A clear band gap in soil can be seen for Configurations 1, 2, and 3, similar in nature to that seen in mortar, but shifted by varying amounts to lower frequencies. Although the band gap narrows slightly, the production of a lower-frequency band gap is desired in designing resonators for the purpose of attenuating seismic waves, which propagate at low-range frequencies. For Configuration 4, the Transmission Ratios for resonators embedded in soil are consistently lower than the Transmission Ratios for resonators embedded in mortar. A band gap is seen at a lower and wider frequency-range for soil.

The results of using the linear elastic soil material indicate the influence of the surrounding material parameters on the band gap. However, soil is not a linear elastic material. It is much more complex, experiencing plastic deformation. The response of soil is also affected by water content, cohesion, friction angle, and many other factors. There are better models available for future studies involving a more realistic soil material. COMSOL Multiphysics [22] includes a built-in soil plasticity model.

Chapter 3

Alternative Resonator Design

Creation of Resonators

Material Selection

Resonators consisting of a heavy metal core and elastic coating have been proven to be effective at attenuating bulk waves. New, improved resonators are designed with this in mind. The resonators target a wide band gap at low frequencies, aiming to effectively attenuate seismic waves. In addition, they are designed with future experiments in mind. Therefore, practical sizing and materials are considered.

The use of a heavy metal core is ideal, as used in the metaconcrete modeling sensitivity analysis. Lead was used in those simulations, which is an extremely dense metal, however it is not practical to use due to safety concerns. The metal core of the new resonators consists of a common engineering material, such as brass or steel. In physical experiments, the simulated bond between the core and thin elastic coating, as well as that between the coating and surrounding material, would be difficult to reproduce. Cylindrical columns are used in the alternative resonator design, replacing the coating of the metaconcrete resonators. The columns, or bars, of an elastic material act as effective springs, allowing the core to resonate properly. Springs themselves could also be used, with a spring constant equivalent to the material properties of the elastic material, however bars were determined as more practical.

In addition, the equally-spaced bars arranged around the core are chosen instead of a coating because this design allows for easy manufacturing of physical models in the form of 3D printing. The material parameters of common 3D-printed plastics are comparable to the nylon and rubber parameters used in the previous metaconcrete simulations, as summarized in *Table 7*.

Table 7 ***Comparison of material parameters of rubber-like materials.***

	Density (kg/m^3)	Young's Modulus (GPa)	Poisson's Ratio
Nylon	1150	1	0.40
Rubber	900	0.01	0.49
Plastic	1200	0.0025	0.4

In Matlack et al. (2016), a polycarbonate lattice with embedded steel cubes, as shown in *Figure 37*, was created and successfully produced band gaps at the design resonant frequencies. The local resonances of the resonators were controlled using geometry [29].

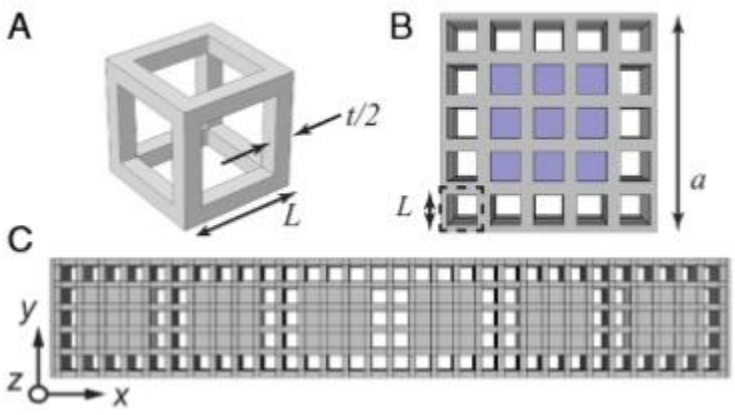

Figure 37 ***Metastructure design from, (a) unit of polycarbonate lattice, (b) unit cell with embedded steel cube, (c) chain of unit cells. Source: Matlack et al. (2016)***

Matlack et al. (2016) serves as an inspiration during the design of the laboratory-scale new, improved resonators. Plastic bars function as springs attached to a heavy metal core. The stiffness of the effective springs is varied by changing the dimensions until the desired theoretical eigenfrequencies are obtained.

Creation of Unit Cell

The unit cell was created in COMSOL Multiphysics [22] and contains a heavy metal core with attached effective springs, embedded in a block. Cylinder-shaped bars are chosen over other shapes for the effective springs because they eliminate sharp edges and are simple to produce. A plastic shell is modeled around the outside of the bars, leaving air voids between them. This shell is very thin and exists to separate the resonators from the material of the block. The sizing of the resonators is determined using an iterative process. The material parameters of the block are set to match those of mortar and soil. A conceptual design of the unit cell is shown in *Figure 38*.

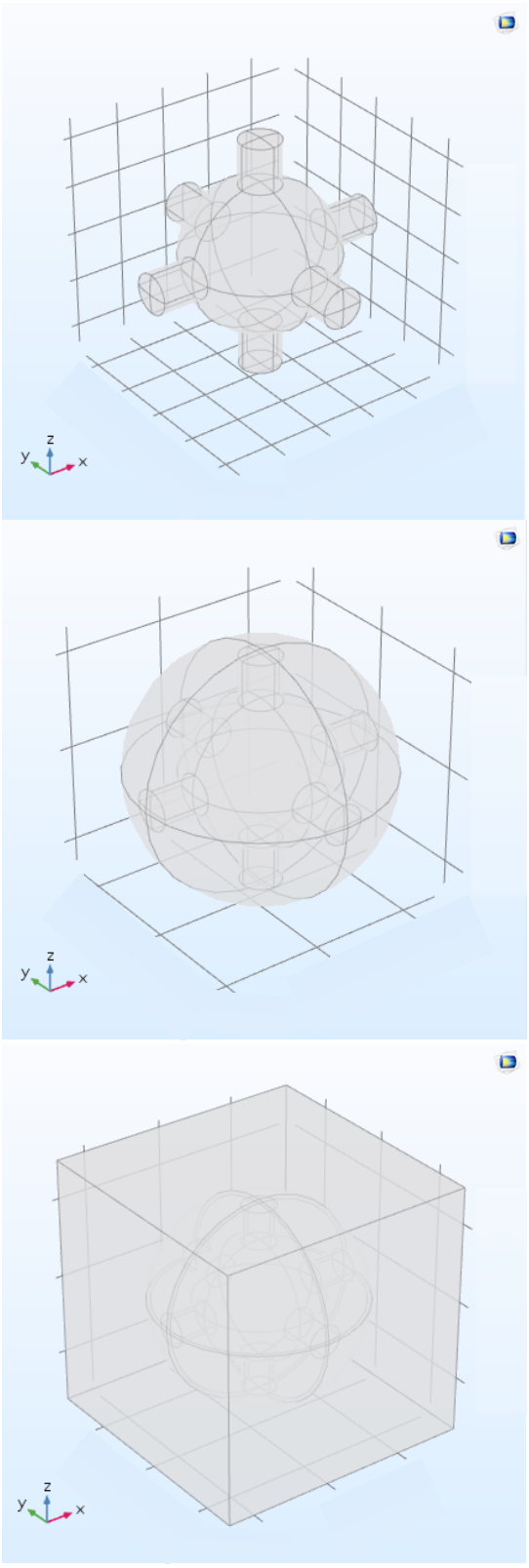

Figure 38 ***Conceptual design of new improved resonators in COMSOL Multiphysics.***

Eigenfrequency Analysis

An eigenfrequency analysis is conducted on the unit cell by applying periodic boundary conditions to lateral faces of the block material. This was done using both soil and mortar as the block material. A comparison of the material properties of mortar and soil is shown in *Table 8*. While many eigenfrequency values can be obtained, the ones of interest are those that produce a mode shape corresponding to rigid body translation of the core. The modal analysis of the alternative resonators, whose size was similar to the metaconcrete resonators, resulted in eigenfrequency values that were approximately 112 Hz, as seen in *Figure 39*. The eigenfrequencies of the metaconcrete unit cell in Chapter 2 were on the scale of approximately 4-20 kHz. The dimensions of the metaconcrete and alternative unit cells are approximately the same size but produce a much different magnitude frequency response. The new, alternative resonators are an improvement because they target lower frequency values, closer to the scale of seismic waves.

Table 8 ***Material parameters of mortar and soil.***

	Density (kg/m^3)	Young's Modulus (GPa)	Poisson's Ratio
Mortar	2500	30	0.2
Soil	1600	0.04	0.32

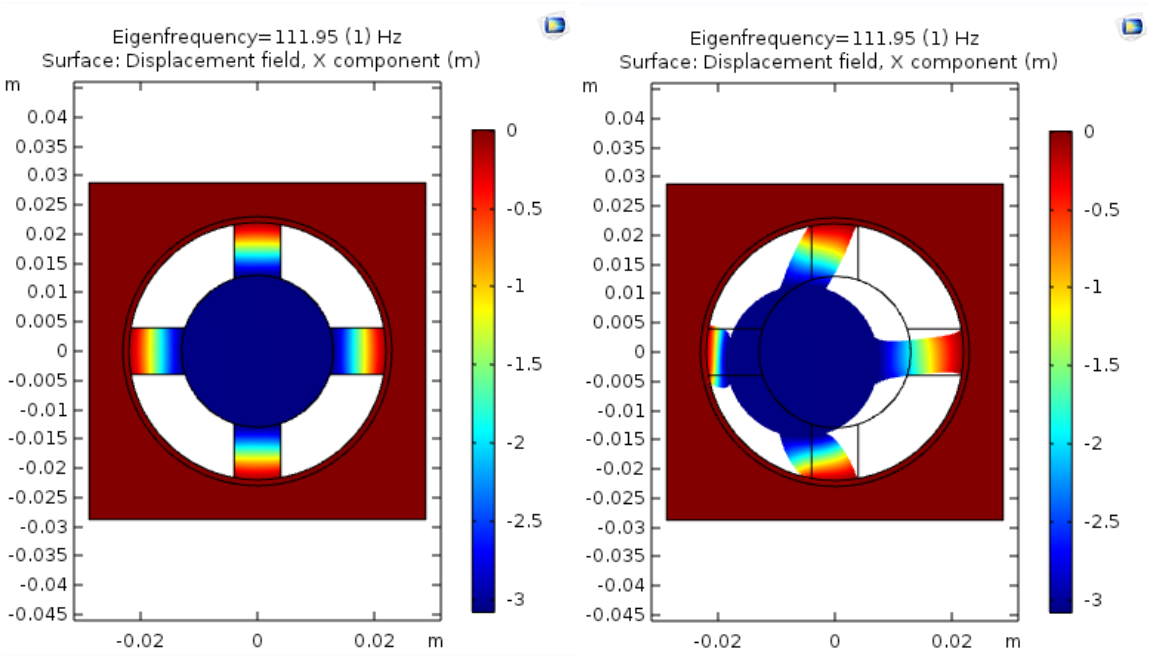

Figure 39 ***Eigenfrequencies demonstrating rigid body translation of core for unit cell of resonators at approximately 112 Hz.***

In the next step, analysis of a slab with repeating resonators, the slab would not be large enough for a full wavelength on the magnitude of 100 Hz, therefore the resonators were scaled up. The final dimensions of the unit cell used in eigenfrequency analysis are summarized in *Figure 40* and *Table 9*.

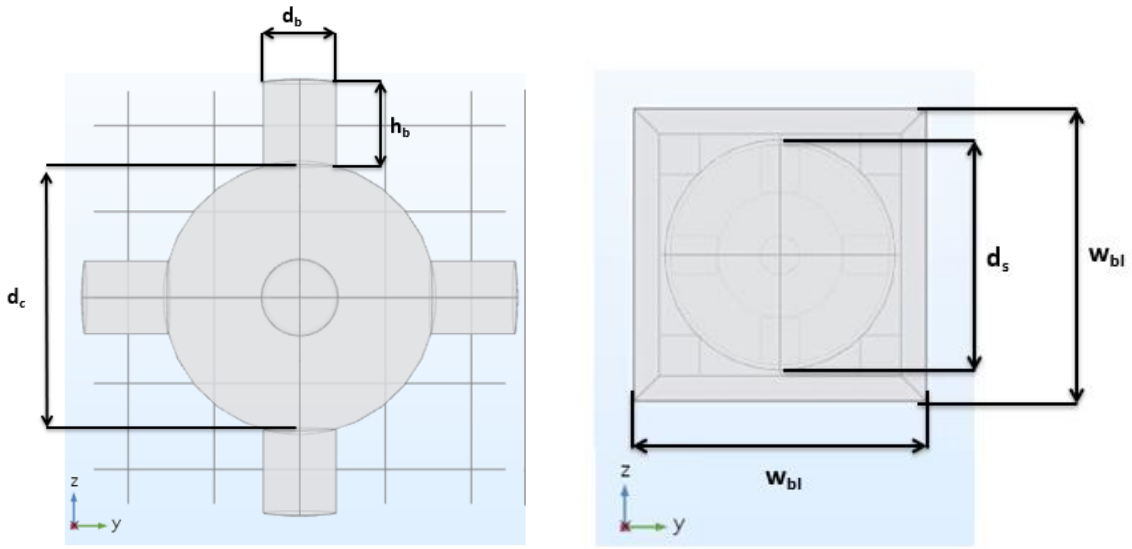

Figure 40 ***Dimensions of unit cell.***

Table 9 ***Dimensional values of unit cell.***

	Label	Value (m)
Diameter of Core	d_c	3
Height of bars	h_b	1
Diameter of bars	d_b	0.8
Diameter of inner shell	d_s	4.8
Shell thickness	t_s	0.1
Width of block	w_{bl}	6.25

The eigenfrequencies of interest obtained from the unit cells in mortar and soil are summarized in *Table 10*, and the desired mode shape produced from modeling the resonators in soil is shown in *Figure 41*.

Table 10 ***Eigenfrequencies corresponding to rigid body translation of core for resonators in mortar and soil.***

	Eigenfrequency 1 (Hz)	Eigenfrequency 2 (Hz)	Eigenfrequency 3 (Hz)
Mortar	1.0217	1.0218	1.0220
Soil	1.0602	1.0603	1.0604

The eigenfrequencies obtained in mortar versus soil are almost the same, therefore all future simulations involving the alternative resonators are performed using soil as the block material, in order to serve as a more realistic model.

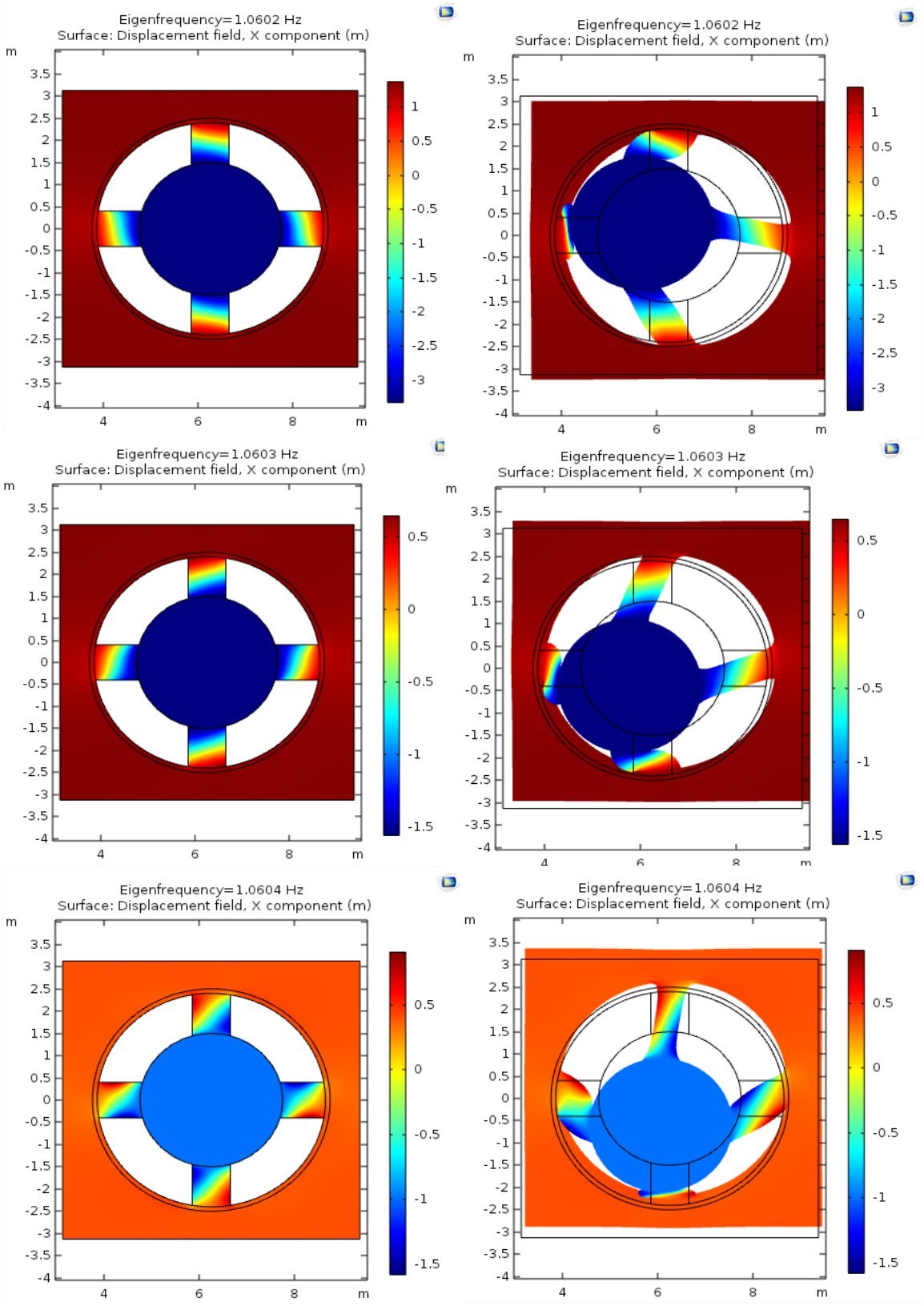

Figure 41 ***Eigenfrequencies demonstrating rigid body translation of core for unit cell of resonators embedded in soil.***

Creation of Slab

In order to perform a sensitivity analysis and tune the band gap produced by the resonators, a slab containing a periodic arrangement of the resonators was created. The resonators are spaced center-to-center at a subwavelength distance. The dimensions of the slab are summarized in *Figure 42* and *Table 11*. The dimensions of the slab in the z-y plane are the same as those in the unit cell, shown in *Figure 40*. For analysis of the slab in the frequency domain, periodic boundary conditions were applied to the lateral faces of the slab. A prescribed displacement was applied to the end face of the slab in the x-direction, and a free boundary condition was applied to the other end face.

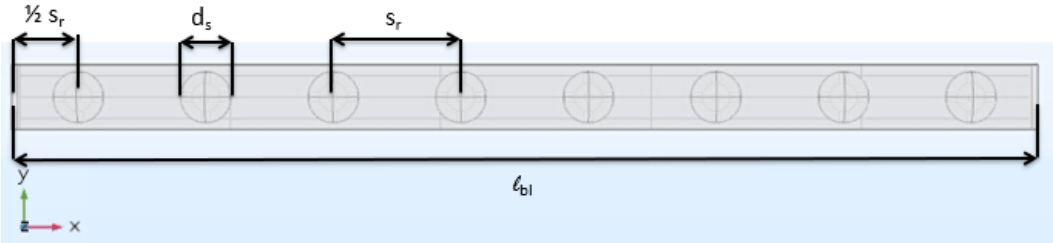

Figure 42 ***Dimensions of slab containing resonators.***

Table 11 ***Dimensional values of slab containing resonators.***

	Label	Value (m)
Spacing of resonators	s_r	12.5
Length of block	ℓ_{bl}	100

Band Gap Widening

The materials, geometry, and density of the resonators are varied and analyzed in an attempt to widen the band gap at the desired frequency range. This proves to be an iterative process, in which influences on the lower bound, upper bound, and width of the band gap are investigated.

Influence of Core Material

The mass of the core is known to be an influence on the resonant frequency of a local resonator. A denser mass should result in a lower-frequency band gap. Therefore, the frequency domain analysis of two different core materials are tested. Brass and steel are common engineering materials that are safe, inexpensive, and available. They are also relatively dense, so they serve as ideal materials for the core of the alternative resonators. The material properties of brass and steel are shown in *Table 12*. From the unit cell eigenfrequency analysis, a band gap is expected around 1 Hz. The results of a frequency domain analysis of the soil slab containing resonators with different core materials are shown in *Figure 43*.

Table 12 ***Material properties of brass and steel.***

	Density (kg/m^3)	Young's Modulus (GPa)	Poisson's Ratio
Brass	8500	100	0.31
Steel	8000	200	0.26

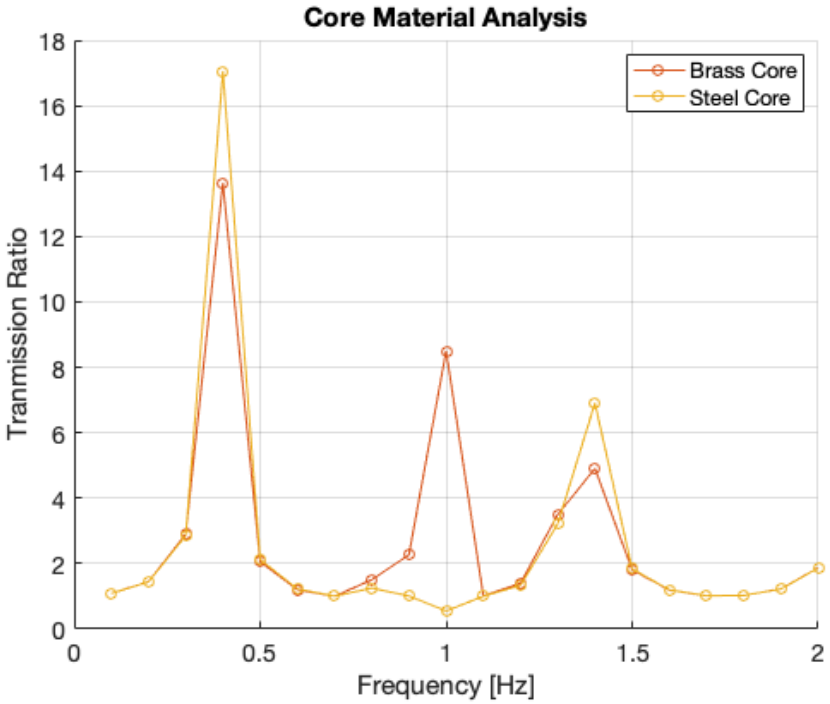

Figure 43 ***Effect of brass vs. steel core material on Transmission Ratio.***

The results for brass and steel are almost the same, with an exception at an eigenfrequency of 1 Hz, where brass has a higher transmission ratio. This disagrees with the expected results, in which a band gap is to be present around 1 Hz, and the band gap for brass is to occur over a slightly lower frequency range than that of steel because of brass' higher density. To further investigate these results, the displacement field across the slab containing resonators with a brass core is plotted at 1 Hz and analyzed. The slab containing the resonators is operating at the correct mode, rigid body displacement of the core, at this frequency, as demonstrated in *Figure 44*. The displacement decreases gradually along the length of the slab, as desired. While the Transmission Ratio at nearby frequencies is lower than at 1 Hz for the brass core, the rigid body translation of the core is effectively reducing the displacement in the slab at this frequency.

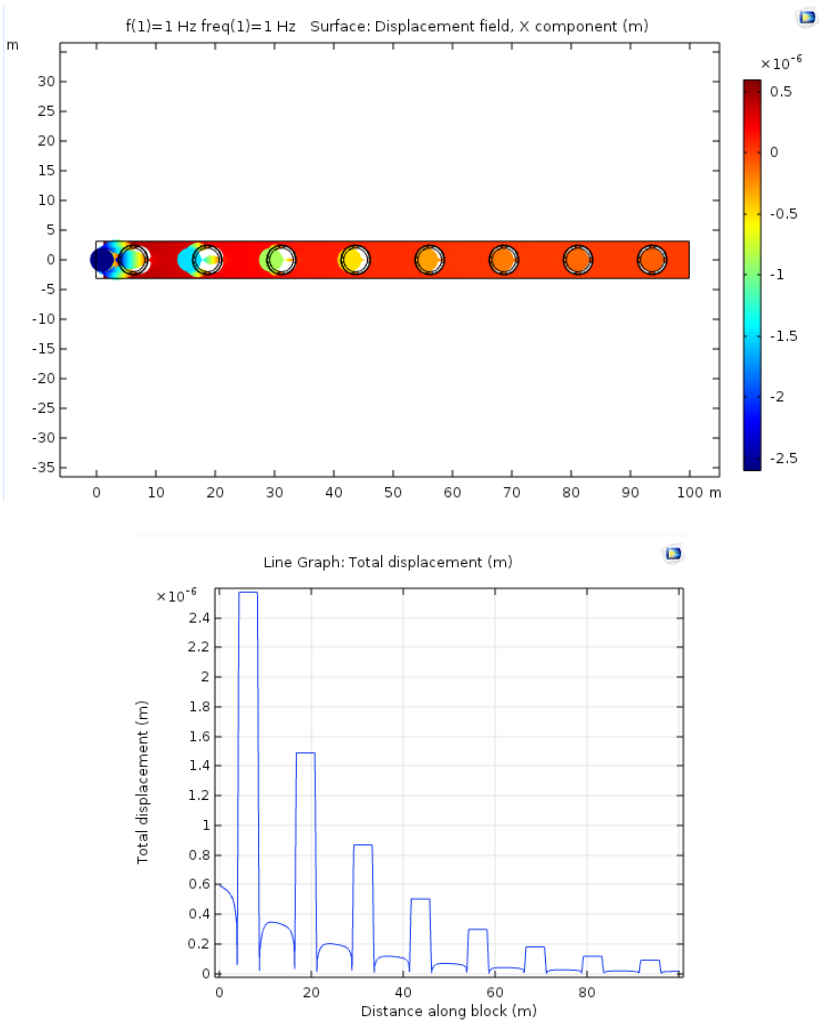

Figure 44 ***Section view of displacement and line graph of displacement vs. length along slab with brass core at 1 Hz.***

A wider range of frequency is investigated in order to determine if there is another band gap present for either core material that was not found in the eigenfrequency analysis. The results are shown in *Figure 45*. For most frequencies from 1-20 Hz, the Transmission Ratio of the slab containing resonators is less than that for the empty soil block.

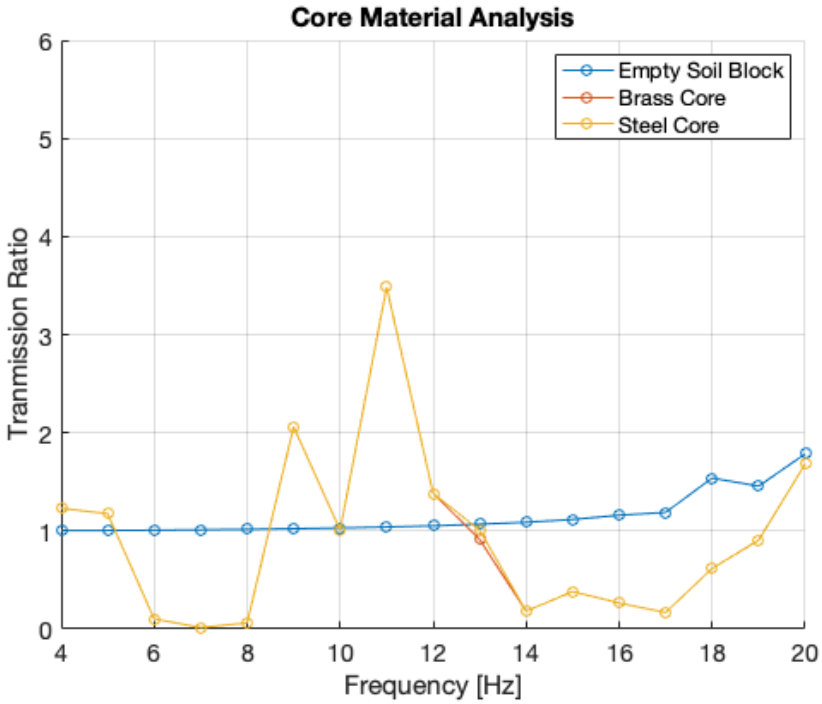

Figure 45 ***Larger frequency range investigation of effect of brass vs. steel core on Transmission Ratio.***

A distinct band gap, where the Transmission Ratio reaches almost zero, is observed from 6 to 8 Hz. Then, another possible band gap occurs from 14-17 Hz. A section view of the displacement field and a line graph of displacement along the length of the slab is shown at 7 Hz in *Figure 46*. At 7 Hz, there is a periodic decrease in the displacement along the length of the slab, as desired. However, the displacement field indicates that this is not due to rigid body translation of the core, but rather another mode. *Figure 47* shows close-up view of the displacement field at this frequency, which looks to activate a flexing or twisting of the bars. A section view of the displacement field at 16 Hz is shown in *Figure 48*, and also indicates that the drop in Transmission Ratio at this frequency is not due to rigid body translation of the core.

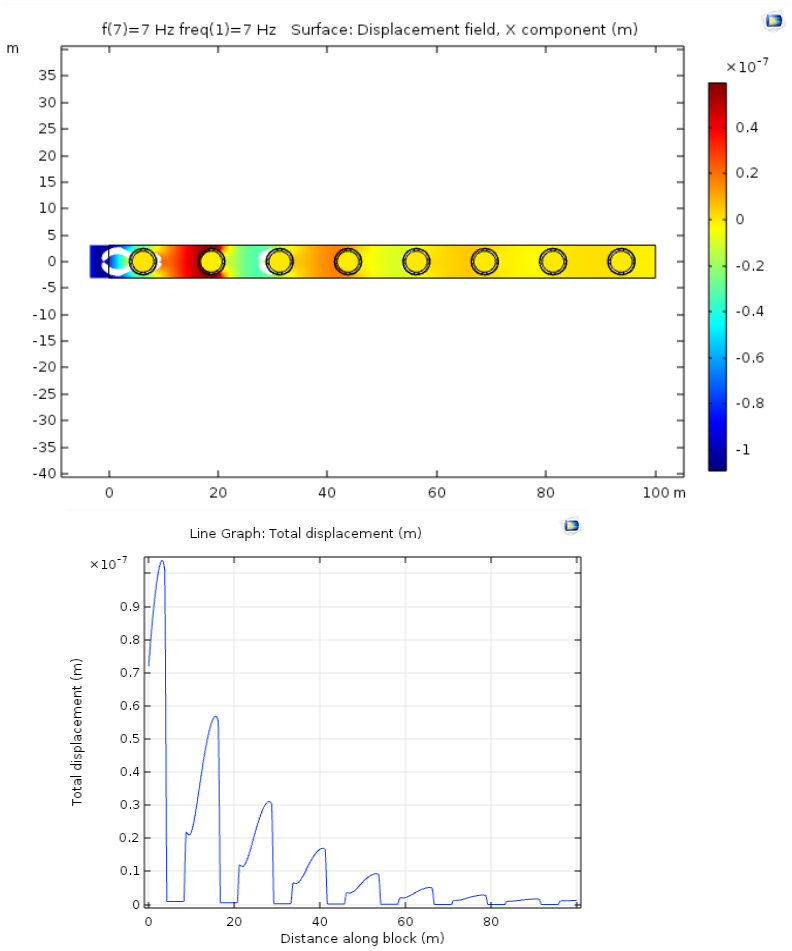

Figure 46 ***Section view of displacement and line graph of displacement vs. length along slab at 7 Hz.***

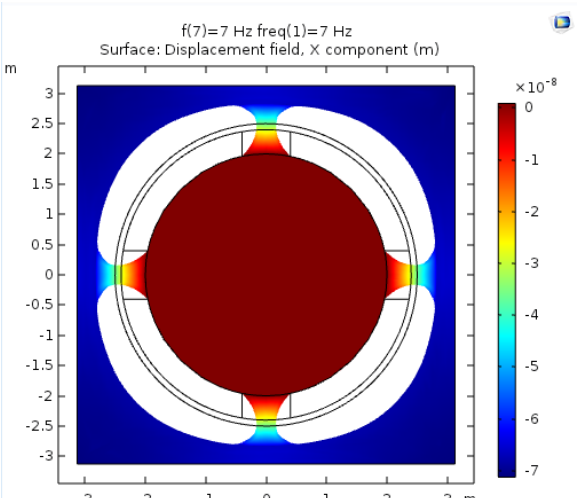

Figure 47 ***Displacement field of single resonator at 7 Hz.***

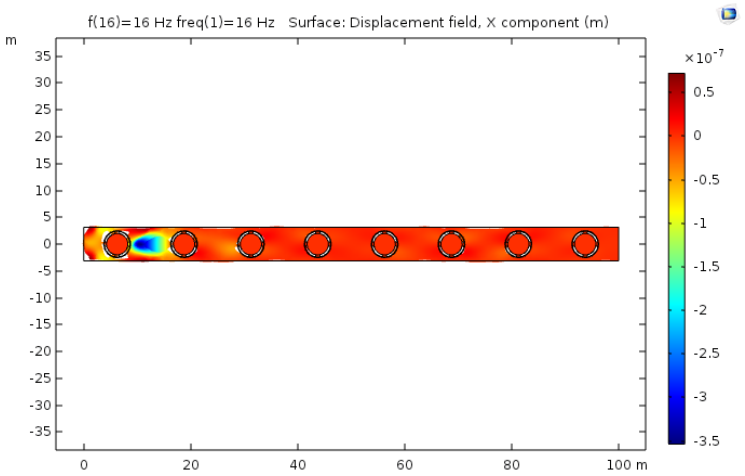

Figure 48 ***Section view of displacement at 16 Hz.***

From 9-12 Hz, the Transmission Ratio for the slab containing resonators is higher than the Transmission Ratio for the empty soil block. As seen in *Figure 49*, the total displacement does not gradually increase along the length of the slab containing resonators at 11 Hz. Resonance of the slab could result in the large jump in Transmission Ratio observed at this frequency.

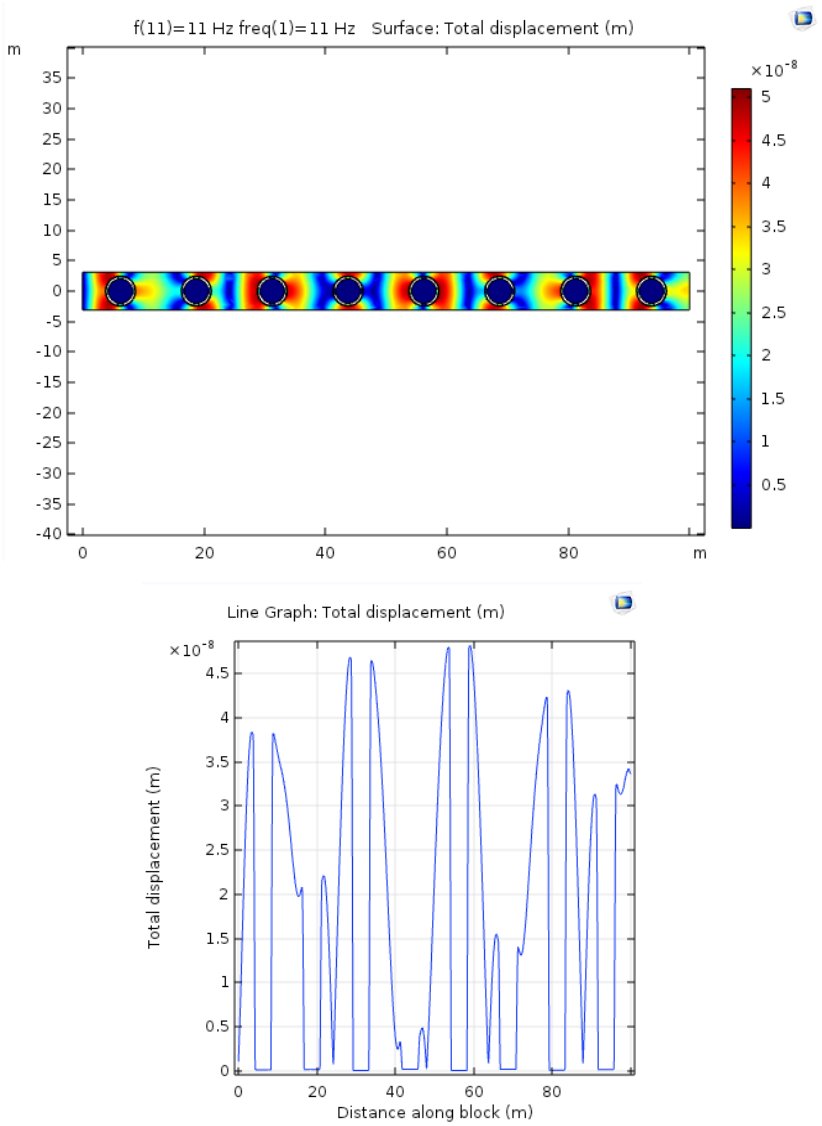

Figure 49 ***Section view of displacement and line graph of displacement vs. length along slab at 11 Hz.***

Analysis of Varying Plastic Stiffness

The stiffness of springs attached to a heavy mass is also known to influence the resonant frequency of a local resonator defined by a mass-spring system. The cylindrical bars in the alternative resonator design act as effective springs. Therefore, changing their height or cross-sectional area

changes the stiffness of the spring-system and may affect the band gap produced by the slab. The stiffness of a bar, k, can be defined by

$$k = \frac{E * A}{L}$$

where E is the elastic modulus of the bar material, A is the cross-sectional area, and L is the length/height of the bar.

First, the result of varying the height of the bars is investigated. The resonator size is kept constant, so when the height of the bars decreases, the radius of the core increases, and vice versa. The original resonator sizing involves a core radius of 1.5 m and a bar height of 1 m, as shown in *Table 9*. The results around the frequency range of interest for increasing the bar height from the original dimension (and simultaneously decreasing the core radius), are shown in *Figure 50*. The results for decreasing the bar height are shown in *Figure 51*.

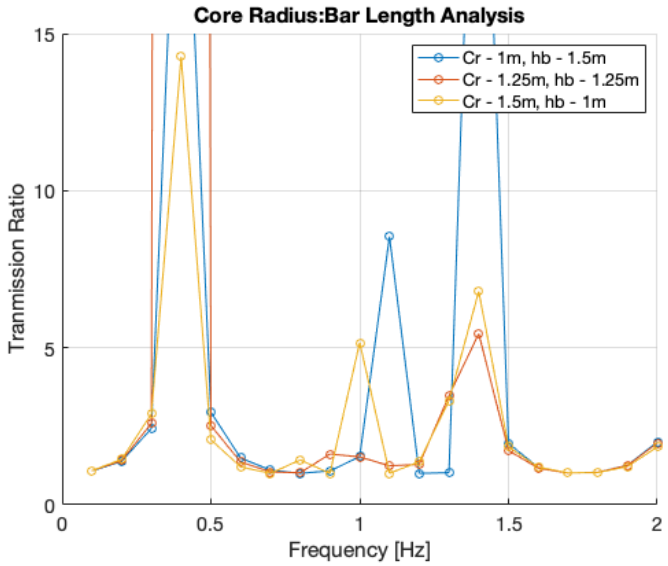

Figure 50 ***Effect of increasing bar height on Transmission Ratio.***

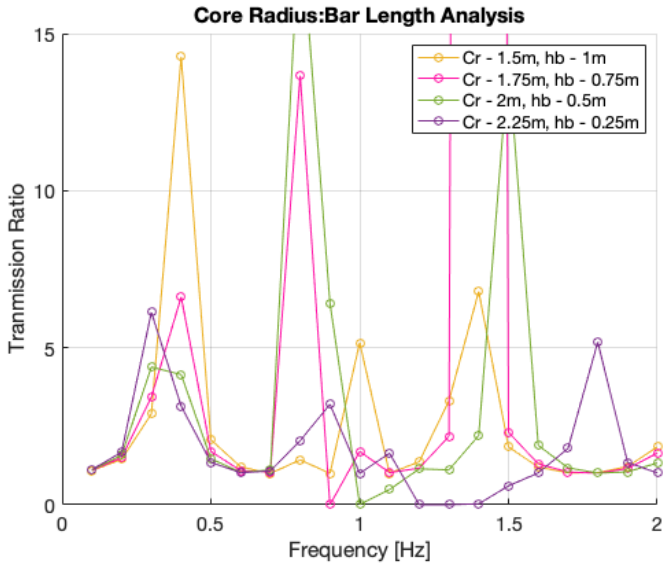

Figure 51 ***Effect of decreasing bar height on Transmission Ratio.***

Increasing the bar height from the original value seems to neither increase nor decrease the Transmission Ratio consistently. However, decreasing the bar height produces a drop in Transmission Ratio around 1 Hz. For bar heights 0.25 to 0.75 m, the frequency of the drop in Transmission Ratio increases with decreasing bar height. The drops occur for only a single frequency for bar heights 0.5 and 0.75 m. The smallest bar height tested, 0.25 m, produces a band gap from 1.2-1.4 Hz. An investigation of the displacement field confirms that at these values, where the Transmission Ratio reaches zero, rigid body translation of the core is occurring.

Varying the bar diameter can also change the stiffness and therefore affect the transmission of the slab containing aggregates. With the original dimensions for the core radius and bar height, the effect of changing the diameter of the bars is analyzed. The transmission plots for decreasing and then increasing the bar diameter from the original dimensions are shown in *Figure 52* and *Figure 53*, respectively.

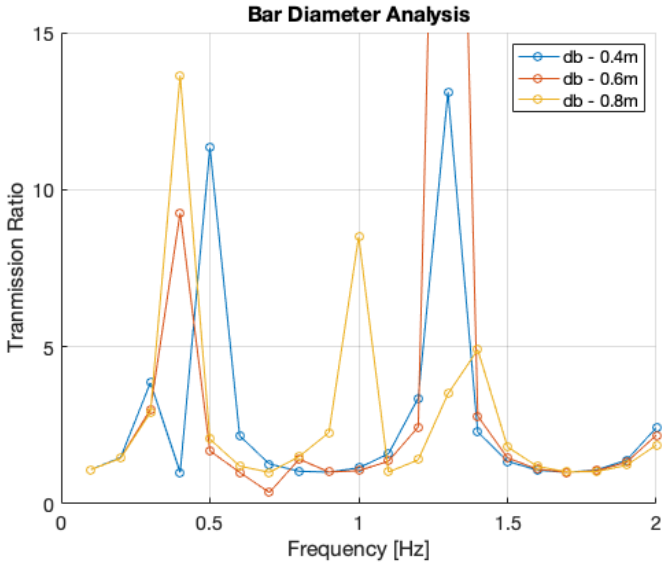

Figure 52 ***Effect of decreasing bar diameter on Transmission Ratio.***

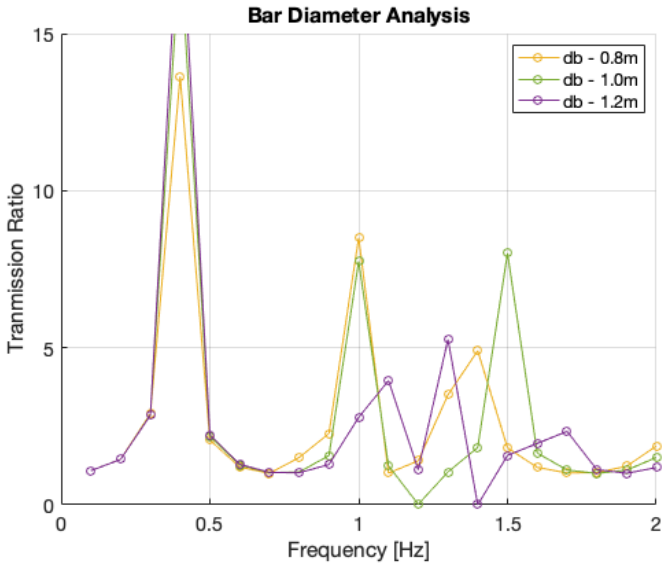

Figure 53 ***Effect of increasing bar diameter on Transmission Ratio.***

Decreasing the bar diameter from the original values of 0.8 m does not produce any additional drop in the Transmission Ratio. For an increased bar diameter, a single-frequency drop is observed. The Transmission Ratio reaches zero at 1.4 Hz for the slab containing resonators with a bar diameter of 1.2 m, and 1.2 Hz for a bar diameter of 1.0 m. The displacement field of the slabs at the frequencies for which the Transmission Ratio drops to zero confirms that rigid body translation of the core is occurring.

These two investigations involving the cylindrical bars that act as effective springs suggest that a larger bar height and smaller bar diameter decrease the frequency at which rigid body translation of the core occurs in the resonators and displacement decreases along the slab. In Matlack et al. (2016), a high, medium, and low stiffness geometry are analyzed. The stiffness is influenced by the number of bars surrounding the mass, where the high stiffness geometry has the most attached bars and the low stiffness geometry has the least. They found that the unit cell with a lower stiffness produced a lower and wider band gap than the unit cells with a medium and high stiffness [29].

The results from varying the plastic stiffness by altering the bar diameter and bar height of the alternative resonators agree with Matlack et al.'s results. A smaller bar diameter and larger bar height decreases the stiffness of the bars, and a lower-frequency drop in Transmission Ratio occurs.

Effect of Increased Density of Resonators

In the analysis of the metaconrete resonators, the slab was originally created with 8 aggregates, and then 28 quarter-spheres were added and the difference in transmission was analyzed. The same is performed for the alternative resonators. 28 quarter-resonators are added along the length of the slab containing 8 full resonators, resulting in 36 total inclusions, as shown in *Figure 54*.

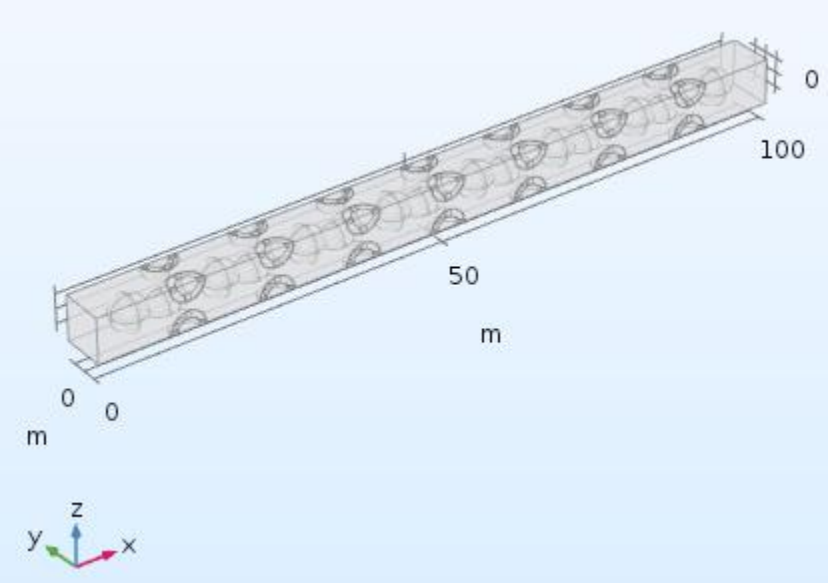

Figure 54 ***Slab with increased resonator density.***

Then, the transmission of the slab with the increased resonator density is plotted, as shown in *Figure 55*. The Transmission Ratio drops to zero, or almost zero, at 0.8 and 1.1 Hz. Both dips are due to

the rigid body translation of the resonator cores. Overall, the more densely-packed slab does not produce significantly advantageous results over the slab containing only eight aggregates.

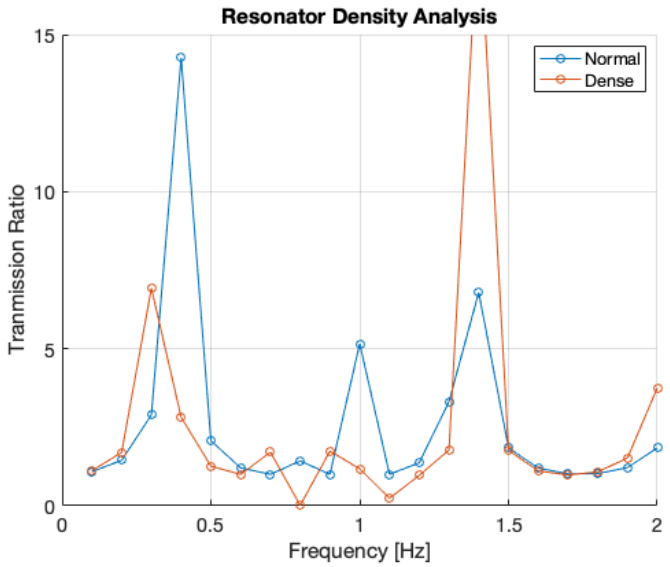

Figure 55 ***Effect of resonator density on Transmission Ratio.***

Summary of Influences on Band Gap

For the slab containing resonators, a drop in the Transmission Ratio to near-zero values was discovered at the expected eigenfrequency, corresponding to rigid body translation of the core. However, the alternative resonator design and sensitivity analysis did not result in the production of a wide band gap at frequencies in the seismic wave range. The density of the core material did not influence the transmission over the frequency range investigated. Varying the plastic stiffness of the resonators by changing the bar diameter and height did not produce consistent results in shifting or widening the band gap. Increasing the number of the resonators in the slab did not significantly decrease the transmission. As previously said, the resonator sizing and subsequent band gap optimization is an iterative process. More investigation is needed in this area. However, the successful activation of the mode of interest at a very low frequency, 1 Hz, is promising.

Chapter 4

Conclusions and Recommendations

The findings of this thesis provide important progress toward the goal of creating a seismic shield using acoustic metamaterials to effectively protect structures from damaging earthquake waves and blasts. Laboratory-scale resonators characterized by bi-material spherical inclusions embedded in a mortar slab, also known as a metaconcrete slab, created band gaps at certain frequencies. Depending on the coating thickness and material, the band gaps were at most 10 kHz wide and fell within the frequency range of 4-30 kHz. Numerical simulation confirmed that a denser core, stiffer coating material, and thicker coating shifted the band gap to lower frequencies. In addition, the use of soil as the block material over mortar created a lower-frequency band gap. The soil was treated as a linear elastic material. However, soil is much more complex in reality. Soil particles experience plastic deformation influenced by water content, cohesion, angle of friction, and more. Additional testing in which the soil is modeled as an elasto-plastic material would more accurately represent the real case scenario and better inform future experiments.

The metaconcrete, originally designed and tested for vertically propagating bulk waves, produced band gaps around the same frequency range when shear waves were applied. For some configurations, the band gap was even widened or shifted to a lower frequency range, both desired results for seismic applications. Additional testing is needed to determine the influences on the band gap produced by the slab subjected to a shear load, however the ability of these resonators to decrease the displacement and therefore damage caused by two different types of seismic waves is extremely advantageous.

A graded array of metaconcrete resonators was able to widen the band gap as compared to a repeating geometry of metaconcrete resonators. The stiffness was varied between subsequent

resonators by changing the thickness of the coating. With more testing, the band gap could be widened even further. Provided resonators designed to reduce transmission within seismic range, the concept of a graded array could be used to create a seismic shield that protects critical infrastructure from most seismic frequencies and therefore damage.

Using the information learned in the metaconcrete testing, alternative resonators were designed as heavy cores with attached cylindrical columns acting as effective springs. The resonators were designed with future experiments in mind, so practical materials and sizing were used. The use of cylindrical bars instead of an elastic coating allows the possibility for bars to be 3D-printed, a recently popular and fast-growing construction method. In addition, the geometry of bars acting as effective springs is an improvement to an elastic coating, as it allows for a simpler way to alter the stiffness of the coating and influence the band gap.

The resonators produced an eigenfrequency at 1 Hz, a value close to the range of seismic waves. The ability to produce a drop in transmission at this low of a frequency is a significant development that addresses a research gap in the field, as most studies design resonators that produce band gaps at frequency ranges well above the typical seismic range. Even at this low eigenfrequency range, the sizing of the alternative resonators tested in numerical simulations is practical for real-world application.

The study of the influences on the band gap of the resonators produced inconclusive results. Dips in the Transmission Ratio were observed at or near the expected value of 1 Hz, however the effect on the band gap of varying the core density, plastic stiffness, and resonator density were inconclusive. This could be due to a few factors. One possible influence is the thin plastic shell separating the resonator from the surrounding material and helping to maintain the air voids between the bars. The shell could inhibit the ability of the rigid body translation of the core to occur

at the eigenfrequency value. Another possible influence is the extremely low frequency range of interest, in which results seem to be inconsistent. In addition, although a mesh size convergence was performed, it is possible that for low frequencies the mesh is not satisfactory for some elements of the resonators.

The ability of the metaconcrete to produce band gaps for bulk and shear waves and the band gap-widening effect of a graded array of bi-material spherical inclusions are promising developments. More work is needed to develop effective alternative resonators that produce a wide band gap, but the ability of a practically-sized geometry to resonate at a low frequency, on the scale of the magnitude of seismic waves, is a feat not many studies have been able to achieve.

The knowledge gained from the testing of both the metaconcrete and alternative resonators in this thesis can be combined to create resonators that can be fine-tuned to produce a wide band gap at low frequencies for two different types of seismic waves. The results of this thesis demonstrate encouraging progress toward the goal of creating a seismic shield capable of protecting a critical structure from damage.

BIBLIOGRAPHY

[1] USGS, Earthquake Statistics, Earthquake Hazards Program. (2016). https://earthquake.usgs.gov/earthquakes/browse/stats.php (accessed October 11, 2018).

[2] E.A. Cavallo, A.P. Powell, O. Becerra, Estimating the Direct Economic Damage of the Earthquake in Haiti, SSRN Electronic Journal. (2010). doi:10.2139/ssrn.1817279.

[3] S.L. Kramer, Geotechnical earthquake engineering, Prentice Hall, Upper Saddle River, N.J., 1996.

[4] H.J. Xiang, Z.F. Shi, S.J. Wang, Y.L. Mo, Periodic materials-based vibration attenuation in layered foundations: experimental validation, Smart Mater. Struct. 21 (2012) 112003. doi:10.1088/0964-1726/21/11/112003.

[5] M. Hadi, M.E. Uz, M.E. Uz, Earthquake Resistant Design of Buildings, CRC Press, 2017. doi:10.1201/9781351200875.

[6] P.A. Deymier, Introduction to Phononic Crystals and Acoustic Metamaterials, in: P.A. Deymier (Ed.), Acoustic Metamaterials and Phononic Crystals, Springer Berlin Heidelberg, Berlin, Heidelberg, 2013: pp. 1–12. doi:10.1007/978-3-642-31232-8_1.

[7] V. Narayanamurti, H. L. Störmer, M. A. Chin, A. C. Gossard, W. Wiegmann, Selective Transmission of High-Frequency Phonons by a Superlattice: The “Dielectric” Phonon Filter, Physical Review Letters - PHYS REV LETT. 43 (1979) 2012–2016. doi:10.1103/PhysRevLett.43.2012.

[8] R. Martínez-Sala, J. Sancho, J.V. Sánchez, V. Gómez, J. Llinares, F. Meseguer, Sound attenuation by sculpture, Nature. 378 (1995) 241. doi:10.1038/378241a0.

[9] Z. Liu, X. Zhang, Y. Mao, Y.Y. Zhu, Z. Yang, C.T. Chan, P. Sheng, Locally Resonant Sonic Crystal, Science. (2000). http://science.sciencemag.org/content/289/5485/1734.full (accessed October 11, 2018).

[10] S. Brûlé, S. Enoch, S. Guenneau, Emergence of Seismic Metamaterials: Current State and Future Perspectives, ArXiv:1712.09115 [Physics]. (2017). http://arxiv.org/abs/1712.09115 (accessed October 11, 2018).

[11] A. Colombi, D. Colquitt, P. Roux, S. Guenneau, R.V. Craster, A seismic metamaterial: The resonant metawedge, Scientific Reports. 6 (2016) 27717. doi:10.1038/srep27717.

[12] A. Colombi, P. Roux, S. Guenneau, P. Gueguen, R.V. Craster, Forests as a natural seismic metamaterial: Rayleigh wave bandgaps induced by local resonances, Scientific Reports. 6 (2016) 19238. doi:10.1038/srep19238.

[13] Z. Shi, J. Huang, Feasibility of reducing three-dimensional wave energy by introducing periodic foundations, Soil Dynamics and Earthquake Engineering. 50 (2013) 204–212. doi:10.1016/j.soildyn.2013.03.009.

[14] S.-H. Kim, M.P. Das, Seismic Waveguide of Metamaterials, Modern Physics Letters B. 26 (2012) 1250105. doi:10.1142/S0217984912501059.

[15] Huang Jiankun, Shi Zhifei, Application of Periodic Theory to Rows of Piles for Horizontal Vibration Attenuation, International Journal of Geomechanics. 13 (2013) 132–142. doi:10.1061/(ASCE)GM.1943-5622.0000193.

[16] Z. Cheng, Z. Shi, Novel composite periodic structures with attenuation zones, Engineering Structures. 56 (2013) 1271–1282. doi:10.1016/j.engstruct.2013.07.003.

[17] S. Brûlé, E.H. Javelaud, S. Enoch, S. Guenneau, Experiments on Seismic Metamaterials: Molding Surface Waves, Phys. Rev. Lett. 112, 133901. (2014). https://journals-aps-org.ezaccess.libraries.psu.edu/prl/abstract/10.1103/PhysRevLett.112.133901 (accessed October 11, 2018).

[18] A. Palermo, S. Krödel, A. Marzani, C. Daraio, Engineered metabarrier as shield from seismic surface waves, Scientific Reports. 6 (2016) 39356. doi:10.1038/srep39356.

[19] M. Miniaci, A. Krushynska, F. Bosia, N.M. Pugno, Large scale mechanical metamaterials as seismic shields, New J. Phys. 18 (2016) 083041. doi:10.1088/1367-2630/18/8/083041.

[20] S.J. Mitchell, A. Pandolfi, M. Ortiz, Investigation of elastic wave transmission in a metaconcrete slab, Mechanics of Materials. 91 (2015) 295–303. doi:10.1016/j.mechmat.2015.08.004.

[21] S. Krödel, N. Thomé, C. Daraio, Wide band-gap seismic metastructures, Extreme Mechanics Letters. 4 (2015) 111–117. doi:10.1016/j.eml.2015.05.004.

[22] COMSOL Multiphysics®, COMSOL Multiphysics® Modeling Software, COMSOL Multiphysics® Modeling Software. (2019). https://www.comsol.com/ (accessed February 10, 2019).

[23] Abaqus, Abaqus Unified FEA - SIMULIA™ by Dassault Systèmes®, Abaqus Unified FEA - SIMULIA™ by Dassault Systèmes®. (2019). https://www.3ds.com/products-services/simulia/products/abaqus/ (accessed February 10, 2019).

[24] FHWA, Chapter 4 - Evaluation of LS-DYNA Soil Material Model 147, Federal Highway Administration Research and Technology. (2004).

https://www.fhwa.dot.gov/publications/research/safety/04094/04.cfm (accessed February 5, 2019).

[25] IOWA DOT, Engineering Properties of Soil and Rock, (2015).

[26] H.S. Yu, CASM: a unified state parameter model for clay and sand, International Journal for Numerical and Analytical Methods in Geomechanics. 22 (1998) 621–653. doi:10.1002/(SICI)1096-9853(199808)22:8<621::AID-NAG937>3.0.CO;2-8.

[27] Y. Wen, G. Yang, Z. Zhong, X. Fu, Y. Zhang, A Similar Cam-clay Model for Sand Based on the Generalized Potential Theory, in: IACGE 2013, American Society of Civil Engineers, Chengdu, China, 2013: pp. 162–169. doi:10.1061/9780784413128.020.

[28] COMSOL, The Geomechanics Module User's Guide, (2013).

[29] K.H. Matlack, A. Bauhofer, S. Krödel, A. Palermo, C. Daraio, Composite 3D-printed metastructures for low-frequency and broadband vibration absorption, Proc Natl Acad Sci U S A. 113 (2016) 8386–8390. doi:10.1073/pnas.1600171113.

Academic Vita of Alexis Gawelko

ang5382@psu.edu

EDUCATION

Bachelor & Master of Science in Civil Engineering — Graduation: May 2019
The Pennsylvania State University, University Park, PA
Schreyer Honors College

SOFTWARE

AutoCAD, Microstation, gINT, MATLAB, COMSOL Multiphysics, LaTeX

TECHNICAL EXPERIENCE

Geotechnical Engineering Intern
Gannett Fleming, Valley Forge, PA — May – Aug. 2018
- Performed stability calculations using estimated soil parameters to ensure safe design of retaining walls and abutments
- Monitored micropile installation, load tests for I-95 replacement project
- Characterized soil samples during drilling and entered data into gINT for further analysis of subsurface profiles

Land Planning & Site Development Intern
The Pidcock Company, Allentown, PA — May – Aug. 2017
- Utilized AutoCAD to design multi-acre sites including lot layout, grading, stormwater management, erosion and sediment control
- Conducted budget estimates for engineering project costs and construction

Highway Design Intern
Johnson, Mirmiran & Thompson, Allentown, PA — May – Aug. 2016
- Assisted highway engineers with several key projects in all stages of implementation from design to construction completion
- Designed roadway improvements, bridge replacements, and traffic patterns

RESEARCH EXPERIENCE

Graduate Researcher
Pennsylvania State University, University Park, PA — 2017-18
- Design and execute experiments to study wave attenuation in meta-soil, with ultimate goal of cloaking structures from earthquakes and blasts
- Present findings at weekly group meetings with interdisciplinary research team
- Perform numerical simulations in COMSOL to model experimental results

LEADERSHIP

Professional Development Lead, Women in Engineering Program — 2018
- Coordinate and instruct professional development session for 170 first-year student participants
- Model positive academic outcomes and career development for students to optimize retention of women in engineering

Vice President, Penn State American Society of Civil Engineers — 2018
- Assist in career fair planning and preparation to host 100+ attending companies
- Implement outreach, career development programs for 200-member chapter

Treasurer, Penn State ASCE Concrete Canoe — 2017-18
- Participate in the technical design, construction, and racing of a concrete canoe
- Direct material procurement and management of club funds

Career Envoy, Penn State Engineering Career Services — 2017-18
- Provide walk-in advising hours to assist engineering students in resume building, interview preparation, professionalism, and career choices

INVOLVEMENT

Vice President, Penn State American Concrete Institute — 2017-18
Traveler, Inaugural Chile Study Abroad Embedded Course — 2017-18
Participant, Penn State Civil Engineering Alumni Mentoring Program — 2016-18
Member, Penn State Society of Women Engineers — 2015-18